

## WHO WE ARE

*The Minnesota Center for Prion Research and Outreach (MNPRO) is a multi-disciplinary center at the University of Minnesota focusing on the biology and epidemiology of human and animal prion diseases and related protein misfolding disorders (PMDs). MNPRO collaborates with a range of University of Minnesota faculty and external team members to conduct research with a broad impact on PMDs, such as Alzheimer's disease, Parkinson's disease, ALS, and emerging PMDs, such as chronic wasting disease.*

## HISTORY

**MNPRO was formed in 2019 with funding support from the Legislative-Citizen Commission on Minnesota Resources, with a mandate to improve diagnostic and surveillance capabilities, and outreach and education on chronic wasting disease (CWD). MNPRO researchers have since made dramatic breakthroughs in testing technology that enable faster and more accurate results, improved methods for detecting prions on a variety of surfaces, and novel outreach approaches to share scientific discovery with a wide public audience.**

## MISSION

Our mission is to become a worldwide hub for combating neurodegenerative disease by utilizing comparative medicine and biology, creating a think-tank environment for cutting-edge science, developing strategic research priorities in the areas of diagnostics and assessment, and collaborating through targeted outreach.



## COLLABORATION

### Hmong

Translations of important resources now available in translation, including Hmong, Spanish, and French; Karen and Khmer/Cambodian coming soon

### Amish

Customized CWD bandana  
Culturally-relevant educational materials for Hunter's Safety class  
Focused, face-to-face engagements

### Native

Engaging Tribal Natural Resource Managers in collaborative partnerships to increase understanding of CWD, and support the creation of Tribal-led disease policies and management

Connecting with underserved minority communities to develop tailored outreach materials to share scientific research in ways that incorporate their cultural values, knowledge, and perspectives.

Learn more at [mnpro.org](http://mnpro.org)





## RESEARCH



### Diagnostic Advancement RT-QulC

Antemortem tissue sample types can be used for CWD diagnosis. Standardized and replicable method for analyzing data Nanoparticle-enhanced RT-QulC.



### Environmental Surfaces & Soil

Developing methods for disinfecting prion contaminated knives and cutting boards. Findings show CWD prions persist in the environment for greater than 15 years.

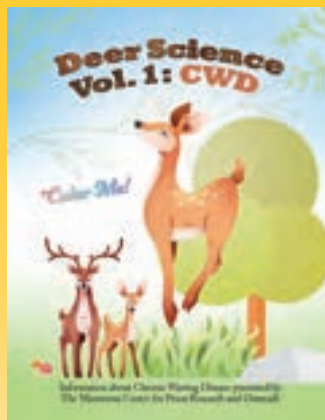


### Educational Advancement 3D Anatomical Models

Conceptualized and developed first of its kind, life-size, 3-D anatomical models of deer and bovine heads as educational aids.



## OUTREACH



# 21,500

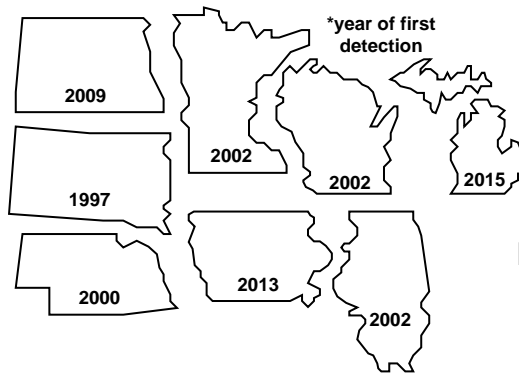
people engaged at targeted events throughout 2023

including:

Minnesota State Fair  
(18,000 visitors to our CWD booth)  
Minnesota Deer & Turkey Classic  
(2,000 hunters and outdoor enthusiasts)  
Fillmore County Fair

Amish community visits  
Student Initiative for Reservation Veterinary Services (SIRVs) clinics  
Tribal Management Plan Community Meetings  
Professional conferences

CWD is a contagious, fatal brain disease affecting wild and farmed deer, elk, moose, and caribou.



CWD is spreading throughout the upper Midwest and has been reported in 30+ states, Canada, Finland, Norway, Sweden, and South Korea.



Virus



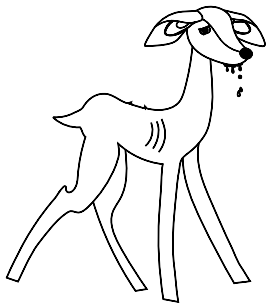
Bacteria

CWD is caused by misfolded prion proteins, not by viruses or bacteria.

There is no vaccine, treatment for, or natural immunity to CWD.

CWD is always fatal.

For a long time, infected deer don't look sick. When they do...



Sick deer become thin, drink and urinate excessively, have poor balance & coordination, lack body fat, have drooping ears, and have difficulty swallowing. This leads to death by pneumonia, predators, hunters, or vehicle collisions.

While a deer is sick, it will spread prions through infected saliva, blood, feces, urine, antler velvet, and eventually, its remains when it dies.

Prions survive for many, many years in the environment.



Experts from the University of Minnesota are currently working on developing faster and more accessible diagnostic tests, researching the way CWD spreads, and analyzing the ecological impacts of the disease.

The Minnesota Department of Natural Resources and the Minnesota Board of Animal Health are surveying and managing CWD in Minnesota and working to limit its spread in wild and farmed cervids across the state.



### Is CWD-positive venison safe to eat?

Take caution! We do not yet know the full risk that CWD poses to humans. Currently there is no direct evidence that CWD poses a risk for humans, but it is important to avoid eating CWD contaminated meat.

## What Can I Do?

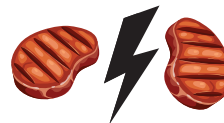


Dispose of deer processing waste responsibly:

1. Use provided dumpsters in CWD zones
2. Use household waste streams going to landfills
3. Leave on landscape where harvested

Minnesota DNR's CWD regulations are an important part of reducing disease spread. Carefully read the regulations prior to every hunting season.





Have your deer processed and wrapped individually so as not to mix CWD-positive and CWD-not-detected venison.

CWD prions can be removed from stainless steel surfaces by using a 1:1 water to household bleach solution and a 5 minute soak. Always follow the appropriate safety precautions when handling bleach.





Have your deer tested, even if it's not mandatory in your hunting zone. Wait to eat your venison until CWD test results are determined to be "not detected."

Keep hunting!  
You are an important part of controlling the spread of CWD by maintaining healthy population numbers.



# What can a **Slinky** teach us about protein misfolding diseases?

**All proteins have a specific 3-dimensional shape.** When correctly folded, their particular conformation, or shape, permits them to function as intended.

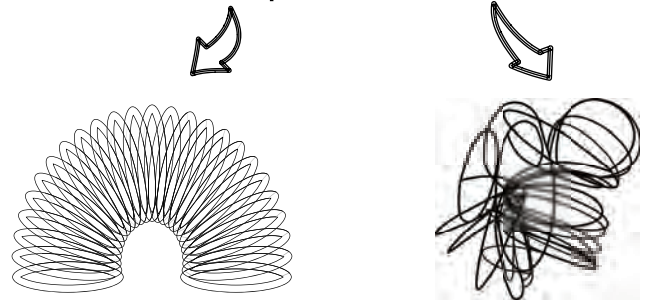
It can be helpful to picture an individual protein as a Slinky. A Slinky has a specific 3D shape. When coiled correctly, a Slinky functions as it's supposed to: it "walks" down stairs. Likewise, correctly-shaped proteins contribute to healthy cellular function.

Slinkys can become tangled, however. A "misfolded" Slinky is no longer a very fun toy. It's still essentially a Slinky, but it does not do what it was designed to do.

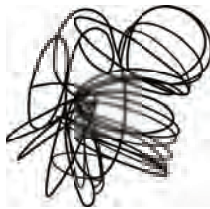
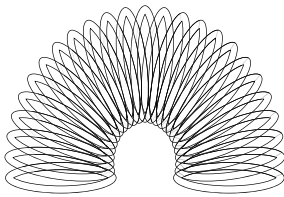
In a process that is not yet well understood, proteins can also undergo a shape change and become misfolded.

Proteins may be pictured like a Slinky because proteins can easily change shape, similar to how Slinkys can stretch and move.

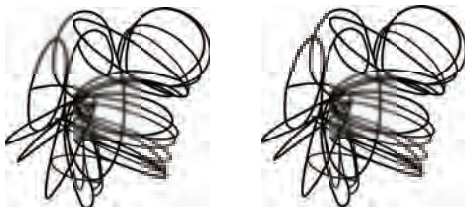
There are healthy proteins and unhealthy proteins.



A healthy protein encounters an unhealthy protein...



It's the same protein, only the shape has changed.



This misfolded protein is the disease-associated form. The healthy protein also becomes misfolded, sparking a chain reaction. As more proteins misfold, plaques form and cells die.

The misfolded form is unable to function correctly. These unhealthy, misfolded proteins can also cause other healthy proteins to misfold and become unhealthy.

Eventually, as misfolded proteins accumulate, they will clump together, forming plaques, which leads to cell death. Because proteins lack genetic material, the body does not recognize the misfolded form as an infection, so it does not mount a substantial immune response.

Misfolded proteins are associated with numerous neurodegenerative diseases in humans and animals, including:

**HUMAN**  
Creutzfeldt-Jakob disease  
ALS  
Alzheimer's  
Parkinson's

**ANIMAL**  
Scrapie (sheep)  
Bovine spongiform encephalopathy (cows)  
Chronic wasting disease (cervids)



UNIVERSITY OF MINNESOTA  
Driven to Discover®

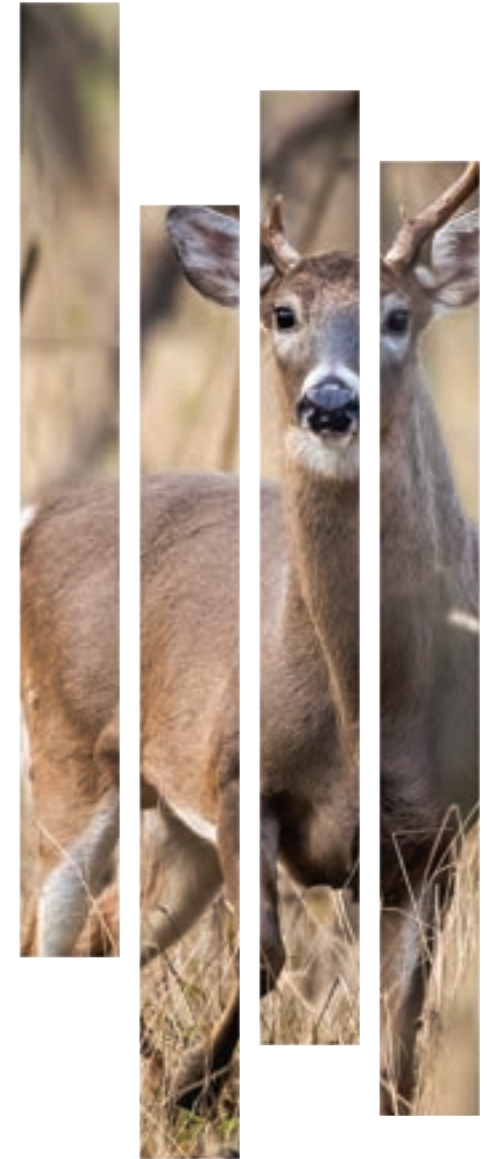


ENVIRONMENT  
AND NATURAL RESOURCES  
TRUST FUND

#### REFERENCES

1. Wilham, J. M., Orrú, C. D., Bessen, R. A., Atarashi, R., Sano, K., Race, B., Meade-White, K., Taubner, L. M., Timmes, A., & Caughey, B. (2010). Rapid End-Point Quantitation of Prion Seeding Activity with Sensitivity Comparable to Bioassays. *PLOS Pathogens*, 6(12), e1001217. <https://doi.org/10.1371/journal.ppat.1001217>
2. Schwabenlander, Rowden, G. R., Li, M., LaSharr, K., Hildebrand, E. C., Stone, S., Seelig, D. M., Jennelle, C. S., Cornicelli, L., Wolf, T. M., Carstensen, M., & Larsen, P. A. (2022). Comparison of Chronic Wasting Disease Detection Methods and Procedures: Implications for Free-Ranging White-Tailed Deer (*Odocoileus virginianus*) Surveillance and Management. *Journal of Wildlife Diseases*, 58(1). <https://doi.org/10.7589/jwd-d-21-00033>
3. Holz, C. L., Darish, J. R., Straka, K., Grosjean, N. L., Bolin, S. R., Kiupel, M., & Sreevatsan, S. (2022). Evaluation of Real-Time Quaking-Induced Conversion, ELISA, and Immunohistochemistry for Chronic Wasting Disease Diagnosis. *Frontiers in Veterinary Science*, 8. <https://doi.org/10.3389/fvets.2021.824815>
4. Burgener, K., Lichtenberg, S. S., Lomax, A., Storm, D. J., Walsh, D. P., & Pedersen, J. A. (2022). Diagnostic Testing of Chronic Wasting Disease in White-Tailed Deer (*Odocoileus virginianus*) by RT-QuIC Using Multiple Tissues. *PLOS ONE*, 17(11), e0274531. <https://doi.org/10.1371/journal.pone.0274531>
5. Tewari, D., Steward, D. L., Fasnacht, M. J., & Livengood, J. (2021). Detection by Real-Time Quaking-Induced Conversion (RT-QuIC), ELISA, and IHC of Chronic Wasting Disease Prion in Lymph Nodes from Pennsylvania White-Tailed Deer with Specific PRNP Genotypes. *Journal of Veterinary Diagnostic Investigation*, 33(5), 943–948. <https://doi.org/10.1177/10406387211021411>
6. Picasso-Risso, C., Schwabenlander, M., Rowden, G. R., Carstensen, M., Bartz, J. C., Larsen, P. S., & Wolf, T. M. (2022). Assessment of Real-Time Quaking-Induced Conversion (RT-QuIC) Assay, Immunohistochemistry and ELISA for Detection of Chronic Wasting Disease under Field Conditions in White-Tailed Deer: A Bayesian Approach. *Pathogens*, 11(5), 489. <https://doi.org/10.3390/pathogens11050489>
7. Ferreira, N., Charco, J. M., Plagenz, J., Orrú, C. D., Denkers, N. D., Metrick, M. A., Hughson, A. G., Griffin, K. A., Race, B., Hoover, E. A., Castilla, J., Nichols, T. R., Miller, M. I., & Caughey, B. (2021). Detection of Chronic Wasting Disease in Mule and White-Tailed Deer by RT-QuIC Analysis of Outer Ear. *Scientific Reports*, 11(1). <https://doi.org/10.1038/s41598-021-87295-8>
8. Li, M., Schwabenlander, M., Rowden, G. R., Schefers, J., Jennelle, C. S., Carstensen, M., Seelig, D. M., & Larsen, P. S. (2021). RT-QuIC Detection of CWD Prion Seeding Activity in White-Tailed Deer Muscle Tissues. *Scientific Reports*, 11(1). <https://doi.org/10.1038/s41598-021-96127-8>
9. Cooper, S. K., Hoover, C. E., Henderson, D. M., Haley, N. J., Mathiason, C. K., & Hoover, E. A. (2019). Detection of CWD in Cervids by RT-QuIC Assay of Third Eyelids. *PLOS ONE*, 14(8), e0221654. <https://doi.org/10.1371/journal.pone.0221654>
10. McNulty, E., Nalls, A. V., Mellentine, S., Hughes, E. K., Pulscher, L. A., Hoover, E. A., & Mathiason, C. K. (2019). Comparison of Conventional, Amplification and Bio-Assay Detection Methods for a Chronic Wasting Disease Inoculum Pool. *PLOS ONE*, 14(5), e0216621. <https://doi.org/10.1371/journal.pone.0216621>
11. Henderson, D. M., Denkers, N. D., Hoover, C. E., McNulty, E., Cooper, S. K., Bracchi, L. A., Mathiason, C. K., & Hoover, E. A. (2020b). Progression of Chronic Wasting Disease in White-Tailed Deer Analyzed by Serial Biopsy RT-QuIC and Immunohistochemistry. *PLOS ONE*, 15(2), e0228327. <https://doi.org/10.1371/journal.pone.0228327>
12. Henderson, D. M., Denkers, N. D., Hoover, C. E., Garbino, N. C., Mathiason, C. K., & Hoover, E. A. (2015b). Longitudinal Detection of Prion Shedding in Saliva and Urine by Chronic Wasting Disease-Infected Deer by Real-Time Quaking-Induced Conversion. *Journal of Virology*, 89(18), 9338–9347. <https://doi.org/10.1128/jvi.01118-15>

## RT-QUIC FACT SHEET



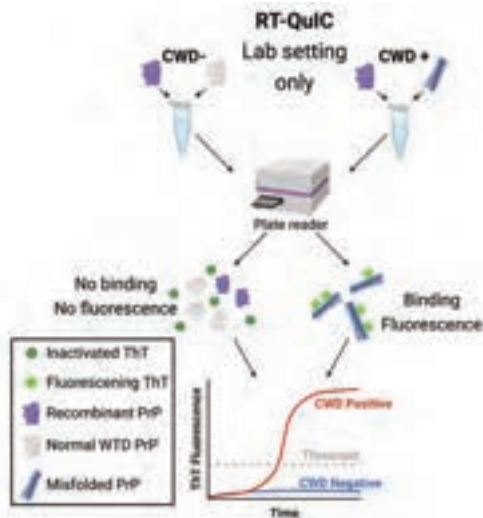
An introduction to the technology  
prepared by the Minnesota  
Center for Prion Research and Outreach

## What is RT-QuIC?

Real-time quaking-induced conversion (RT-QuIC) is a test that is used to diagnose various neurodegenerative diseases in humans and animals.<sup>1</sup> Misfolded protein, or “prion,” diseases include Creutzfeldt-Jakob disease (CJD), Alzheimer’s disease, and Parkinson’s disease in humans; and scrapie in sheep and goats, bovine spongiform encephalopathy (BSE or “mad cow disease”) in cattle, and chronic wasting disease (CWD) in cervids (deer, elk, moose, caribou, and reindeer).

Over the past decade, RT-QuIC has routinely been shown to be a powerful test for detecting prions across a variety of tissue types.<sup>2-5, 7-9, 11, 12</sup>

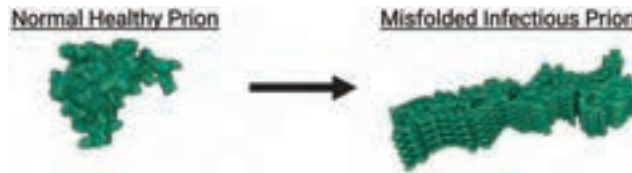
RT-QuIC is a highly sensitive and specific diagnostic tool that can help diagnose these disorders early.



## How Does RT-QuIC Work?

A key feature of prion diseases is the abnormal folding of prion proteins. These misfolded shapes eventually begin to form plaques, killing brain and other nerve cells. The RT-QuIC test works by combining samples of suspect tissues with a synthetic, healthy version of the prion protein. The mixture undergoes cycles of shaking (quaking) and heat. If misfolded prions are present in the tissue sample, this causes the normal prions to misfold, essentially replicating the disease progression process in the body, only much faster and not infectious. The conversion is measured using thioflavin T—a fluorescent dye that works like a molecular magnet—which binds to misfolded prion proteins and produces a light signal when beamed with a laser.

CWD is caused by the misfolding of a normal prion protein into an abnormal, infectious form that kills nerve cells.



RT-QuIC has the potential to detect prions in a variety of sample types.

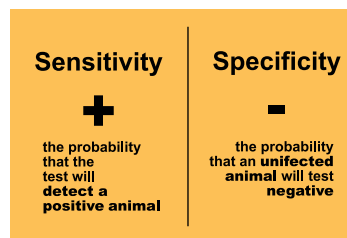


## How Useful is RT-QuIC for Monitoring CWD?

RT-QuIC can identify CWD in deer months before it can be detected by traditional tests, with test sensitivity (i.e. the probability of detecting misfolded prions in an infected deer) ranging from 72% to 96% and test specificity (i.e. the probability that an uninfected deer will test negative) ranging from 91% to 100%.<sup>2-9, 11</sup>

Furthermore, whereas other diagnostic tests are primarily performed post-mortem, RT-QuIC is useful for screening both live and deceased cervids and cervid by-products, including: brain, obex, lymph nodes, tonsils, rectal biopsies, eye tissues, skin, blood, saliva, urine, and feces.<sup>2-5, 7-12</sup> The method can be used not only on freshly deceased animals, but also on animals that are found dead and are at varying stages of decomposition.

A number of research teams across the United States, including MNPRO, are working diligently to internally validate RT-QuIC as a diagnostic tool for CWD using various tissues and biological samples. The USDA is simultaneously investigating the validation of RT-QuIC as a regulatory test.



## How Does RT-QuIC Compare to Other Diagnostic Tools?

There are a number of tests that can be used to diagnose prion diseases. The current tests used by regulatory agencies (e.g. USDA) are antibody-based tests, such as ELISA and IHC. These tests are time-consuming, require expensive equipment, are primarily used post-mortem, and cannot identify misfolded prions during early stages of the disease. RT-QuIC overcomes several of these limitations.

Several peer-reviewed studies have directly compared RT-QuIC performance to ELISA and IHC. **These studies show that the RT-QuIC test provides magnitudes greater sensitivity than the current regulatory tests,<sup>2, 3, 6, 9-11</sup> with low rates of false-positives and false-negatives.** RT-QuIC is incredibly sensitive and can detect even tiny amounts of CWD prion proteins, therefore enabling disease diagnosis at even earlier stages of infection.<sup>11</sup>

In May of 2023, the Michael J. Fox Foundation announced that RT-QuIC can be used to detect Parkinson’s in the cells of living people.

## What Are the Limitations of RT-QuIC?

No test is perfect. Since RT-QuIC is still a relatively new assay, and only a handful of research and diagnostic labs have access to the method, it has not yet been fully validated and formally recognized by the USDA. It requires formal validation before it can be widely adopted for regulatory CWD diagnostics. In order to be validated, the test needs to be shown to routinely detect “true positives” and “true negatives” with a high degree of confidence. It is essential that state and national-level validation of RT-QuIC occur before the test can be widely adopted for official CWD surveillance.

Another limitation of RT-QuIC is that the assay requires a special ingredient—a recombinant “normal” prion protein that is cultured using bacteria in a lab. Few institutions have the infrastructure required to mass-produce the recombinant prion protein required for RT-QuIC. Because it is difficult to mass-produce, this ingredient is not widely available. This is a major limitation for national-level adoption of RT-QuIC and for this reason the MNPRO team is working to solve the recombinant prion protein mass-production issue. MNPRO has successfully developed and made commercially available this necessary ingredient for RT-QuIC assays. *MNPROtein* has been recognized by the USDA, and others, as a huge success in advancing critical research on protein-misfolding diseases, including CWD.



# SURFACE DECONTAMINATION

## FOR CHRONIC WASTING DISEASE



Chronic wasting disease prions can be found in CWD-positive meat and will readily stick to other surfaces, especially steel.

MNPRO researchers have studied various disinfecting agents to determine their effectiveness for removing chronic wasting disease prions from surfaces like stainless steel knives and plastic cutting boards.

Porous materials, like knives with wooden handles and wooden cutting boards, are not recommended for processing venison because they cannot be decontaminated.

Sponges should be thrown away after each use.



Dish soap and Briotech are **NOT effective** for removing CWD prions from hard surfaces.



**Virkon S**  
2% solution

**Effective and recommended** for removing CWD prions from hard surfaces.

Prepare disinfectant solution (it can be used multiple times, but it should be prepared fresh daily).

Remove large matter from surfaces.

Use a 5-minute soak.

Thoroughly rinse and dry.



**Bleach**  
10% or 40%  
solution

**Effective and recommended** for removing CWD prions from hard surfaces.

Prepare disinfectant solution (it can be used multiple times, but it should be prepared fresh daily).

Remove large matter from surfaces.

Use a 5-minute soak. Avoid soaking steel in bleach for more extended lengths of time.

Thoroughly rinse and dry.



The Minnesota Center for Prion Research & Outreach

For more information about this study or about chronic wasting disease, please contact us at [mnpro@umn.edu](mailto:mnpro@umn.edu).



# Nanoparticle-Enhanced RT-QuIC (Nano-QuIC) Diagnostic Assay for Misfolded Proteins

Peter R. Christenson, Manc Li, Gage Rowden, Peter A. Larsen,\* and Sang-Hyun Oh\*



Cite This: *Nano Lett.* 2023, 23, 4074–4081



Read Online

ACCESS |



Metrics & More



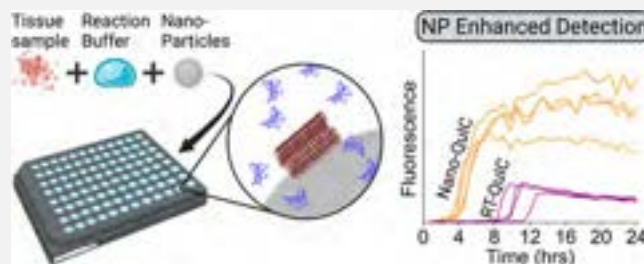
Article Recommendations



Supporting Information

**ABSTRACT:** Misfolded proteins associated with various neurodegenerative diseases often accumulate in tissues or circulate in biological fluids years before the clinical onset, thus representing ideal diagnostic targets. Real-time quaking-induced conversion (RT-QuIC), a protein-based seeded-amplification assay, holds great potential for early disease detection, yet challenges remain for routine diagnostic application. Chronic Wasting Disease (CWD), associated with misfolded prion proteins of cervids, serves as an ideal model for evaluating new RT-QuIC methodologies. In this study, we investigate the previously untested hypothesis that incorporating nanoparticles into RT-QuIC assays can enhance their speed and sensitivity when applied to biological samples. We show that adding 50 nm silica nanoparticles to RT-QuIC experiments (termed Nano-QuIC) for CWD diagnostics greatly improves the performance by reducing detection times 2.5-fold and increasing sensitivity 10-fold by overcoming the effect of inhibitors in complex tissue samples. Crucially, no false positives were observed with these 50 nm silica nanoparticles, demonstrating the enhanced reliability and potential for diagnostic application of Nano-QuIC in detecting misfolded proteins.

**KEYWORDS:** amyloid, prions, RT-QuIC, protein misfolding, gold nanoparticle, silica nanoparticle



Pathological amyloids formed by misfolded proteins (MPs) are found in many human and animal neurodegenerative diseases, including Alzheimer's Disease (misfolded  $A\beta$  and tau), Parkinson's disease (misfolded  $\alpha$ -synuclein), and prion diseases (misfolded cellular prion proteins, PrP<sup>C</sup>).<sup>1–4</sup> Amyloid formation originates via the misfolding of functional proteins into insoluble and degradation-resistant amyloid fibrils that are rich in  $\beta$ -sheet structures. A notable feature across the spectrum of neurodegenerative disease is that the production and deposition of affiliated MPs typically begin years before the onset of clinical symptoms. Consequently, developing highly sensitive diagnostic methods for detecting MPs during presymptomatic stages of neurodegenerative diseases is a critical research area.<sup>5–8</sup> If successful, such methods could facilitate the strategic enrollment of patients in clinical trials and the deployment of therapeutic interventions during the earliest stages of neurodegenerative disease.

Current diagnostics for MP diseases are limited.<sup>9,10</sup> Conventional assays rely heavily on antibody-based enzyme-linked immunosorbent assays (ELISA) and immunohistochemistry (IHC) technologies, which are expensive and time-consuming and require substantial training and expertise to operate.<sup>9</sup> Additionally, antibodies used in these assays often fail to differentiate between native and misfolded proteins due to poor specificity, necessitating protein digestion to enrich MPs. This approach can affect diagnostic sensitivity through the destruction of particular MP-associated strains.<sup>11</sup> Together, these antibody-based assays are limited in the identification of

early stage MPs and are primarily used on tissues collected post-mortem. Real-time quaking-induced conversion (RT-QuIC) has emerged as one of the most promising assays for early diagnosis of various MP-related neurodegenerative diseases.<sup>5,6,9,12,13</sup> Briefly, in RT-QuIC, small volumes of biological samples (e.g., lymph nodes, cerebral spinal fluid, skin, etc.) are seeded into a solution containing an excess of recombinant protein substrate (e.g., recombinant hamster prion protein [rHaPrP]) that, in the presence of a specific MP template, begins to misfold and form amyloids after a period of shaking and incubation. A fluorescent dye Thioflavin T (ThT) then binds to the misfolded substrate protein, yielding a detectable signal based on the basis of light excitation. If MPs are absent in the original biological seed, then misfolding of the substrate protein does not occur, allowing for a clear distinction between the presence or absence of MP-induced amyloid. Amyloid formation in RT-QuIC generally follows sigmoidal kinetics partitioned into three distinct phases—nucleation, growth, and stationary phases—corresponding to particular molecular mechanisms that dominate the RT-QuIC

**Received:** March 15, 2023

**Revised:** April 22, 2023

**Published:** April 26, 2023



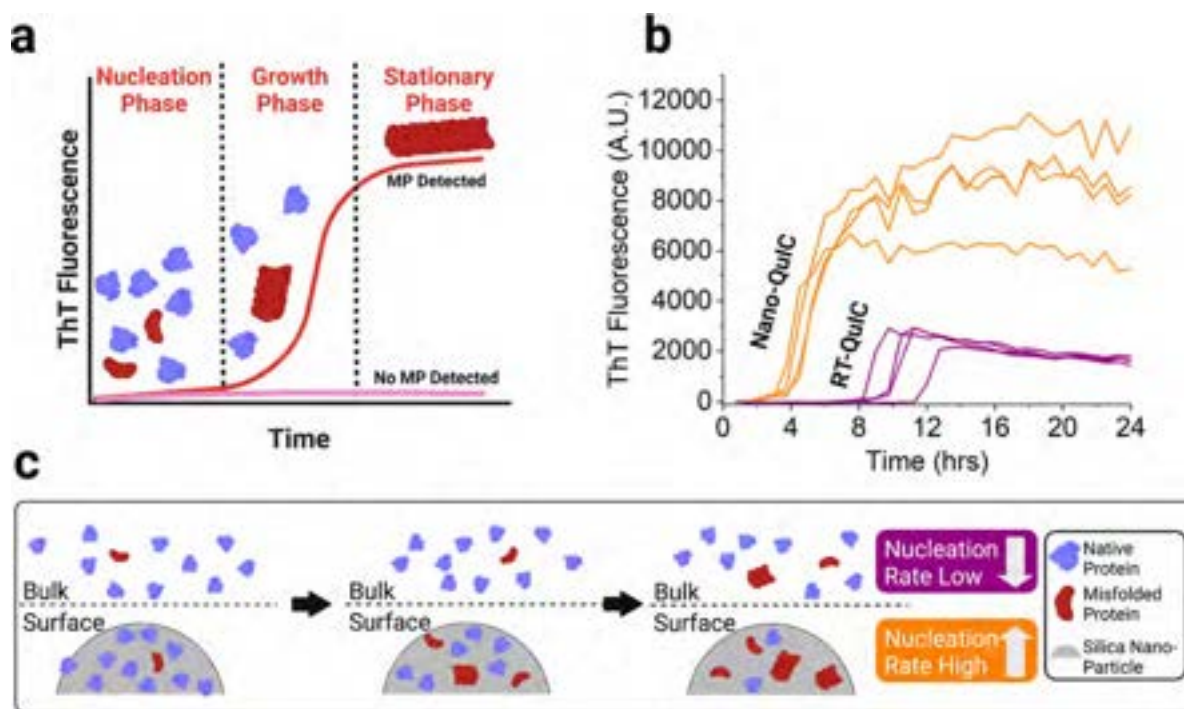


**Figure 1.** (a) Summary of fibril growth under normal conditions (no nanoparticles) showing nucleation, growth, and stationary phases. Sigmoidal curve represents MP detection, and flat line represents no MP detection. (b) Results from Nano-QuIC and traditional RT-QuIC. (Nano-QuIC conditions: 48 °C, 2.5 mg/mL 50 nm silica NPs). (c) Schematic of the Nano-QuIC seeded-amplification mechanism. In Nano-QuIC, silica NPs promote primary nucleation at a higher rate than bulk solution methods such as RT-QuIC.

reaction (Figure 1A). While RT-QuIC has been successfully applied to detect several MPs associated with a variety of neurodegenerative diseases (e.g., TDP-43, Tau, Alpha-synuclein, infectious prions, etc.)<sup>6,13</sup> the complexity of biological samples still poses challenges for clinical diagnostic applications. For example, the assay has low kinetic efficiency, often taking up to 48 h to complete a standard test. Additionally, although it is more sensitive than conventional protein detection methods (i.e., ELISA and immunohistochemistry),<sup>14</sup> natural inhibitors present within biological samples can interfere with reaction kinetics, producing false-negative results.<sup>7,12,15,16</sup> To harness RT-QuIC's potential for early neurodegenerative diseases diagnosis, it is imperative to develop novel methodologies that enhance assay performance, especially diagnostic sensitivity, and facilitate the transition of RT-QuIC from basic research to clinical application.

Chronic wasting disease (CWD), a prion disease affecting cervids across North America, Scandinavia, and South Korea,<sup>17–20</sup> involves the misfolding of cellular prion protein (PrP<sup>C</sup>) into amyloid fibrils by CWD prions (PrP<sup>CWD</sup>), similar to the protein misfolding processes observed across the neurodegenerative disease spectrum. Due to growing concerns about potential interspecies transmission<sup>13,21</sup> PrP<sup>CWD</sup> is one of the most extensively studied MP diseases using RT-QuIC, with several protocols developed to improve assay performance for PrP<sup>CWD</sup> detection.<sup>7,9,13,15,22</sup> Additionally, samples of CWD from animals are more easily obtained than samples from humans. Therefore, PrP<sup>CWD</sup> serves as an ideal model MP for exploring and evaluating novel RT-QuIC methodologies.

Nanoparticles (NPs) have been used to advance diagnostics in a variety of fields<sup>4,23–28</sup> and have been studied extensively for their roles in protein misfolding.<sup>29–37</sup> When proteins adsorb onto a nanoparticle's surface, the local concentration of

the substrate increases, and protein conformation can be altered.<sup>35–38</sup> This can lead to the promotion of nucleation events, which shortens the nucleation phase (Figures 1A, B). While the effects of NPs on the kinetics of amyloid formation have been characterized for several proteins,<sup>29–36</sup> NPs have not been used in RT-QuIC protocols for the detection of MPs in complex biological samples.

In the present study, we applied silica NPs (siNPs) as reagents in RT-QuIC reactions to enhance the detection of CWD prions in lymphoid tissues of wild white-tailed deer. We selected nanoparticles with diameters below 100 nm, as previous research has demonstrated their potential to increase aggregation for various proteins.<sup>29–31,33–36</sup> SiNPs were chosen as the primary focus because they are negatively charged and thus readily interact with the positively charged rHaPrP substrate. Moreover, siNPs are more cost-effective than other NP options, such as gold nanoparticles, thus leading to a more practical application. However, we also explored the performance of gold NPs to demonstrate the versatility and broad applicability of various nanoparticle types in enhancing the RT-QuIC detection of misfolded proteins in biological samples.

We observed that the RT-QuIC performance was significantly improved in the presence of siNPs, corresponding to siNP size. By exploring various combinations of NP diameters, concentrations, and reaction temperatures, we identified optimal RT-QuIC conditions represented by the highest rate of amyloid formation (RAF, see methods, Figure 1B) and the lowest false-positivity rate. We found that the addition of 50 nm siNPs optimized the RT-QuIC performance by significantly increasing both the rate of amyloid formation and ThT fluorescence (Figure 1B). Using sigmoidal-like curves, we fit the kinetic fluorescent data and extracted key parameters that describe the lag time of the nucleation phase and the time

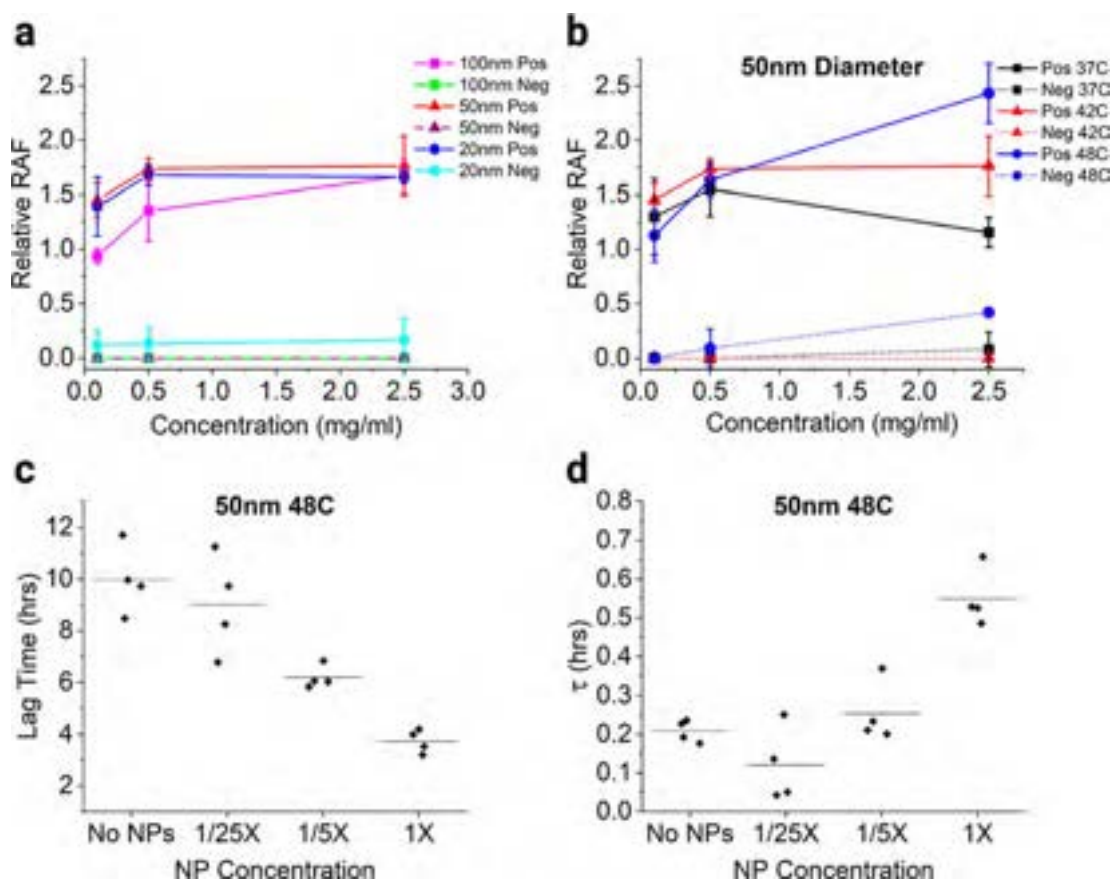


**Figure 2.** (a) Relative rate of amyloid formation (RAF) of various diameter and concentrations of silica NP solutions amplified at 42 °C seeded with CWD positive or negative tissue homogenates. (b) Relative RAF of solutions seeded with CWD positive or negative tissue with various concentrations of 50 nm silica NPs amplified at different temperatures. (c) The lag time of the nucleation phase vs concentration of 50 nm silica NPs at 48 °C. (d) The time constant of fibril growth ( $\tau$ ) vs concentration of 50 nm silica NPs at 48 °C. Unless noted otherwise, error bars show standard deviation.

constant of the growth phase. Our findings reveal that much of the speed increase is likely due to a higher nucleation rate of MP on the siNP surface compared to the bulk solution (Figure 1C). Furthermore, we demonstrated that the accelerating effects of NPs are not just limited to siNPs but can also occur by incorporating gold nanoparticles (AuNPs) in the RT-QuIC reaction. To test whether RT-QuIC with siNPs could overcome effects of inhibitors, we serially diluted CWD-positive lymphoid tissues and found that siNP-enhanced RT-QuIC can readily detect the presence of CWD prions at a concentration previously unattainable. Collectively, our results strongly indicate that the nanoparticle-enhanced RT-QuIC reaction, termed Nano-QuIC, vastly improves diagnostic performance.

## RESULTS

**Effects of siNP Diameter and Concentration on RT-QuIC Performance.** To examine the effects of nanoparticles on RT-QuIC performance, siNPs with diameters ranging from 20 to 100 nm were added as a reagent to RT-QuIC reactions seeded with CWD positive or negative tissue homogenates (parotid lymph nodes). Concentrations of siNPs were set at 0.1, 0.5, and 2.5 mg/mL. Reactions were run for 48 h at 42 °C. All diameters of siNPs examined herein affected the rate of amyloid formation (RAF, see the Supporting Methods) when compared to the RAF of reactions having no siNPs (Figure 2a). The ratio between the RAF of reactions with and without

siNPs gives a parameter known as the relative RAF. For all siNP diameters, the relative RAF increased as the concentration of the siNPs increased (Figure 2a). This led to an average time to CWD detection of 6.3 h (95% confidence interval [CI]:  $\pm 0.96$  h) for 50 nm siNPs at 42 °C, 4.9 h faster than traditional RT-QuIC reactions of the same sample (average time to detection of 11.2 h (95% CI:  $\pm 1.00$  h)). Importantly, the optimal siNP reaction parameters for diagnostic assessment of PrP<sup>CWD</sup> positive tissues examined herein (50 nm siNPs at 42 °C) yielded no false positives.

**Temperature Effects on Nano-QuIC Sensitivity and Specificity.** The temperature of RT-QuIC experiments directly influences their sensitivity and specificity.<sup>39</sup> Higher temperatures typically yield higher RAFs, however, such conditions increase the risk of spontaneous misfolding of the substrate protein. Lower temperatures give lower RAF values, extending diagnostic time and potentially leading to false-negative results but decreasing false-positivity rates. To identify optimal conditions that maximize Nano-QuIC sensitivity and specificity, experiments were performed at 37 °C, 42 °C, and 48 °C for 20–100 nm siNPs with concentrations ranging from 0.1–2.5 mg/mL (Figure 2b and Figure S1). Once again, the relative RAF was found by comparing reactions with and without siNPs. For reactions at 37 °C, all diameters of siNPs led to higher relative RAFs of CWD-positive samples vs the same samples tested with traditional RT-QuIC (Figure 2b and Figure S1). However, compared with siNP experiments

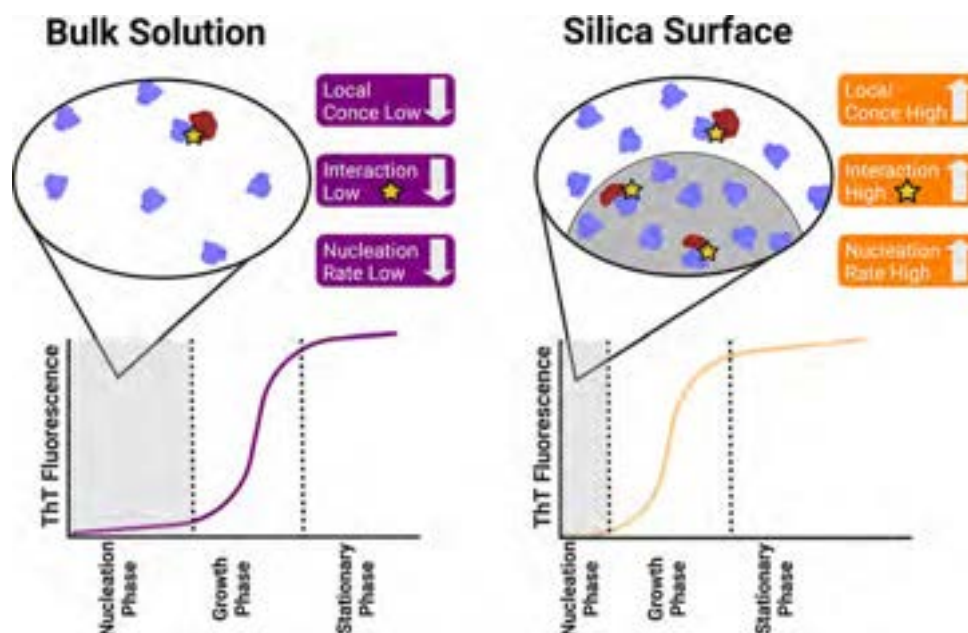


**Figure 3.** Schematic illustration of the proposed mechanism of action. In the bulk solution, RT-QuIC substrate is not concentrated and the number of interactions between misfolded protein and substrate is low. In proximity to the silica surface (Nano-QuIC), the local concentration of substrate is increased, partly due to electrostatic attraction and thus the interactions between misfolded protein and substrates are increased.

performed at higher temperatures, CWD-positive reactions performed at 37 °C exhibited slower RAFs. For Nano-QuIC experiments performed at 48 °C, all diameters of siNPs again led to a higher relative RAF (Figure 2b and Figure S1). Additionally, experiments performed at 48 °C had shorter detection times (higher raw RAFs) compared with reactions at lower temperatures. Nano-QuIC performed using 50 nm siNPs at 2.5 mg/mL and a temperature of 48 °C gave the largest relative RAF and the fastest detection time, just 4.1 h (95% CI:  $\pm 0.45$  h) compared to 10.1 h (95% CI:  $\pm 1.44$  h) for traditional RT-QuIC, a 2.5 $\times$  improvement (Figure 2b). No false positive replicates were observed across our CWD-negative samples (Discussion). Using these parameters, Nano-QuIC was performed on a blinded set of 10 CWD positive and 10 CWD negative wild white-tailed deer retropharyngeal lymph nodes, and all tissues were classified with 100% sensitivity and specificity (Table S1).

**Characterization of Aggregation Kinetics and Mechanism in Nano-QuIC.** The formation of fibrils is a process in which misfolded proteins interact with one another to form large linear structures. Modeling fibril formation in RT-QuIC is achieved using three phases: nucleation (lag), growth (elongation), and stationary<sup>37,40,41</sup> (Figure 1a). The nucleation phase involves native proteins misfolding into nuclei units with low fluorescence values because ThT fluoresces when bound to fibrils<sup>42</sup> and not to single monomers. In the elongation phase, nuclei act as templates to efficiently misfold other native proteins, ultimately producing linear fibrils. In the presence of mechanical shaking or sonication, these fibrils can break, thus creating additional nuclei for native proteins to misfold and making more fibrils. The elongation phase is characterized by exponential growth of fibrils as documented by exponential growth of ThT fluorescence (Figures 1a and 2b). In the final phase, the stationary phase, ThT fluorescence ceases to increase exponentially and stabilizes. This model accounts for both the propagation of infectious prions observed in transmissible spongiform encephalopathies (e.g., CWD or

Creutzfeldt-Jakob disease) as well as the misfolding and spread of proteins associated with various neurodegenerative diseases (e.g., Parkinson's, ALS, and Alzheimer's disease).<sup>30–32,40,41,43</sup>

The three phases of protein amplification using RT-QuIC are modeled using sigmoidal-like curves.<sup>40,41</sup>

$$Y = y_i + m_i x + \frac{y_f + m_f x}{1 + e^{-[(x-x_0)/\tau]}} \quad (1)$$

where  $y_i$  and  $m_i$  are associated with the initial ThT fluorescence and slope of the nucleation phase.  $y_f$  and  $m_f$  are associated with the final ThT fluorescence and the slope of the stationary phase. The time to 50% of the maximum ThT fluorescence is  $x_0$  and  $\tau$  is the time constant for fibril growth. The length of the nucleation phase, which is approximately the time to detection, is given by the lag time,  $x_0 - 2\tau$ .

To characterize the kinetics of how siNPs influence RT-QuIC reactions (50 nm siNPs at 48 °C), eq 1 was used to develop fits that yielded semiquantitative values of lag time and the time constant for fibril growth ( $\tau$ ) for all concentrations (Supporting Methods). We observed a decrease in lag time with increasing siNP concentration (Figure 2c), indicating their crucial role in initial nuclei formation for fibrillation.<sup>43</sup>

At pH 7.4, the RT-QuIC substrate rHaPrP is positively charged, whereas siNPs are negatively charged, leading to an attractive force.<sup>26</sup> This likely promotes the adsorption of rHaPrP onto siNP surfaces, increasing the local effective concentration of the QuIC substrate (Figure 3). Additionally, infectious prions can adsorb onto glass and silica surfaces.<sup>44</sup> Adsorbed proteins can diffuse across the surface and interact with one another.<sup>37,42</sup> Because the local concentration of proteins on the siNP surface is higher than in the bulk reaction space,<sup>35,36,43</sup> there is more opportunity for RT-QuIC substrate to interact with misfolded protein seeds, thus influencing reaction kinetics by facilitating a more efficient nucleation phase. Additionally, proteins adsorbed onto surfaces often change their conformation.<sup>37,38</sup> These changes could make rHaPrP more susceptible to misfolding in the presence of prion

seeds, thus increasing the nucleation rate. It should be noted that the three characteristic phases of protein amplification discussed above were entirely absent from the negative samples.

The time constant for fibril growth ( $\tau$ ) is used to compare fibril growth phases between different RT-QuIC reaction conditions. For 50 nm siNPs at 48 °C, we observed that a higher nanoparticle concentration resulted in longer  $\tau$  (Figure 2d). Additionally, the maximum ThT fluorescence of solutions with NPs was larger than solutions without NPs (Figure 1b). This observation could be accounted for if the siNPs, in the presence of mechanical shaking, are more efficiently breaking the fibrils into smaller units.<sup>37</sup> A greater number of fibril nuclei will recruit more hPrP substrate, thus contributing to an exponential growth phase. Such a mechanism would explain the unique sigmoidal curves observed in Nano-QuIC.

**Nano-QuIC with Gold Nanoparticles.** To demonstrate that acceleration effects of NPs on RT-QuIC performance can apply to other NP types, additional experiments were conducted using AuNPs. Fifteen nanometer citrate-capped AuNPs were added as reagents to RT-QuIC reactions to obtain final concentrations of 20.75, 62.5, or 187.5  $\mu\text{g/mL}$  AuNPs. CWD-positive or CWD-negative tissue homogenates were added to the solutions and RT-QuIC reactions ran for 48 h at 42 °C. RAFs were higher for all solutions containing AuNPs compared to RAFs of reactions without AuNPs (Figure 4). The fastest average time to detection was found to be 8.2 h (95% CI:  $\pm 1.21$  h) compared to the average time of detection of the no AuNP solutions: 12.5 h (95% CI:  $\pm 1.26$  h).

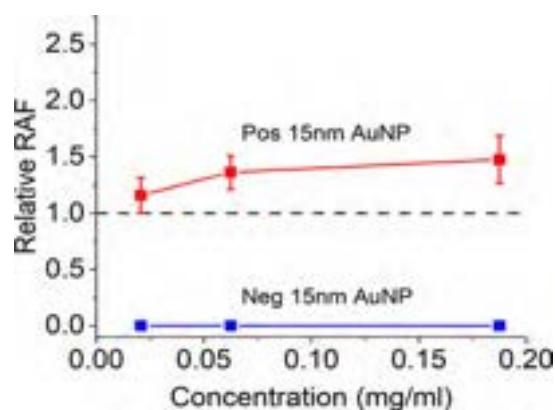


**Figure 4.** Relative RAF (ratio of the RAF of reactions with 15 nm AuNPs compared to those without). Assay was run at 42 °C. Error bars show standard deviation.

**Enhancing Sensitivity and Overcoming Inhibitors with Nano-QuIC.** Tissue dilution series experiments were performed for 50 nm siNPs at 42 °C to compare the sensitivity of Nano-QuIC and traditional RT-QuIC. 10-fold dilutions of CWD-positive tissue seeds were created from  $10^{-1}$  to  $10^{-9}$ . Subsamples of these dilutions (i.e., seeds) were then added to both the Nano-QuIC and traditional RT-QuIC reactions. Nano-QuIC and traditional RT-QuIC detected seeding activity in reactions with seeds diluted to  $10^{-9}$  and  $10^{-8}$ , respectively, documenting the diagnostic sensitivity of these assays. However, for less dilute seeds, Nano-QuIC greatly outperformed traditional RT-QuIC. At dilutions of  $10^{-1}$  PrP<sup>CWD</sup> positive tissue, traditional RT-QuIC exhibited no seeding activity, whereas Nano-QuIC clearly detected the presence of

PrP<sup>CWD</sup> as reflected by high RAF values (Figure 5a, b). Moreover, for PrP<sup>CWD</sup> positive tissue dilutions of  $10^{-2}$ , Nano-QuIC yielded double the RAF yield compared to traditional RT-QuIC (Figure 5a).

Biological samples, especially from clinical settings, are extremely complex, thus making diagnostics challenging.<sup>24,25,27,28,45</sup> Similar to inhibitors that negatively impact PCR performance, RT-QuIC is susceptible to inhibitors that hamper detection and/or the misfolding of protein substrates.<sup>7,12,15,46</sup> Hypothesized RT-QuIC inhibitors include mucin family proteins and polar lipids<sup>7,46</sup> although a variety of inhibitory factors likely exist. Traditionally, RT-QuIC inhibitors are overcome by diluting tissue samples, and concordantly reaction-limiting compounds, until diagnostic sensitivity performs as expected for true-positive samples. However, both inter- and intraindividual MP heterogeneity, as well as stage of neurodegenerative disease (i.e., early vs late stages), directly influence the quantity of MPs present within a given biological sample. Therefore, the practice of diluting diagnostic samples to overcome inhibitors may contribute to the production of false-negatives<sup>45</sup> (i.e., the diagnostic samples are true positives, yet have very low levels of MPs that are subsequently diluted below the limit of detection). Our data indicate that Nano-QuIC has the potential to overcome false-negatives associated with sample dilution and/or inhibitors, as the siNP-improved assay exhibited 100% sensitivity in replicates where traditional RT-QuIC failed (Figure 5). In light of the hypothesized operational mechanism for Nano-QuIC (described above, see Figure 1C), we posit that the protein substrate (rHaPrP) binds to the siNP surface, thus increasing the local rHaPrP concentration and allowing for more efficient interaction with MPs and subsequent misfolding. This overcomes inhibitors and ultimately improves diagnostic sensitivity.

## DISCUSSION

This study shows that incorporating siNPs into RT-QuIC reactions, forming Nano-QuIC, can greatly accelerate the time to detection of a prion disease (4.1 h, a 2.5 $\times$  improvement). To the best of our knowledge, this is the first report of NPs being used as reagents for RT-QuIC-based diagnostics with biological samples. By analyzing kinetic data, we observed acceleration of the nucleation phase and longer growth phase time constants for reactions with SiNPs.<sup>35</sup> To demonstrate the effects of other NPs, Nano-QuIC was performed with 15 nm AuNPs, an experiment that revealed AuNPs influence RT-QuIC reaction kinetics similar to siNPs. Importantly, our results indicate Nano-QuIC overcame tissue-associated inhibitor effects and significantly outperformed traditional RT-QuIC for detecting MPs at higher tissue concentrations (Figure 5a, b).

We observed that RT-QuIC reactions performed with 50 nm siNPs and a run temperature of 48 °C yielded optimal diagnostic conditions, resulting in no false positives and up to a 2.5 $\times$  improvement of time to diagnosis. For this condition, the negative sample's fluorescence rise slightly due to siNPs increasing background fluorescence; however, the kinetic curves of negative control samples do not exhibit the characteristic exponential fibril growth phase, indicating that CWD-negative reactions are not seeding or creating fibril nuclei (Figure S2). The kinetic curves of diagnostic negative samples produced by Nano-QuIC are clearly distinguishable from true-positives.

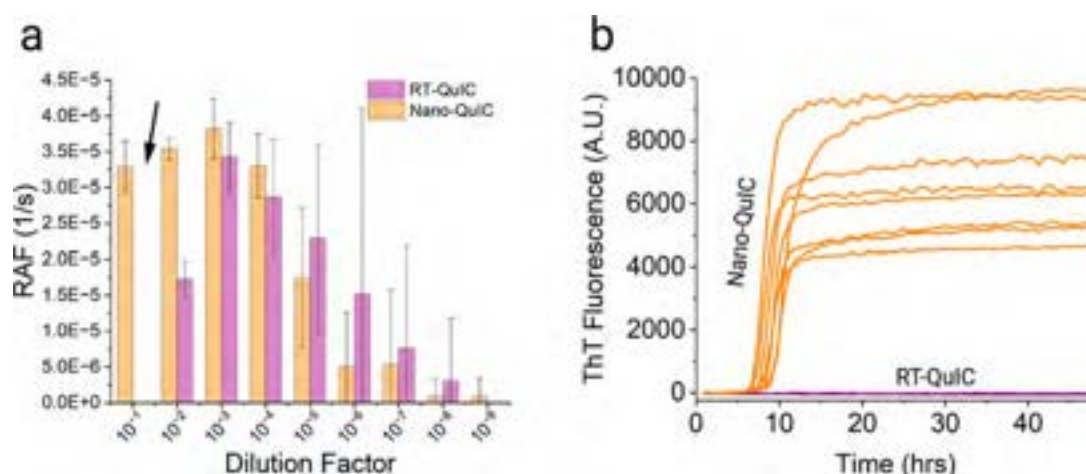


**Figure 5.** (a) Raw RAF for a 10-fold dilution series of CWD positive tissue amplified at 42 °C in RT-QuIC vs Nano-QuIC (50 nm siNPs, 2.5 mg/mL). Arrow highlights the lack of signal (false negative) from RT-QuIC, likely due to inhibitors. (b) Kinetic curves for  $10^{-1}$  CWD positive tissue dilution amplified at 42 °C in RT-QuIC versus Nano-QuIC (50 nm siNPs, 2.5 mg/mL). Unless noted otherwise, error bars show standard deviation.

Previously, NPs have been studied for their roles in promoting or preventing spontaneous amyloid formation<sup>29–36</sup> and structural impacts of amyloids. However, our work demonstrates the diagnostic potential of NPs for determining the disease status of complex biological samples, which has not been explored before. Although large, near-millimeter-scale beads have been used in RT-QuIC,<sup>47–50</sup> they did not achieve the diagnostic performance seen with siNPs in this study.

We have shown the utility of Nano-QuIC for lymph node tissue samples, which are commonly used by wildlife agencies for CWD detection. Future research on larger sample sets is needed for epidemiological validation. In addition, antemortem diagnostic applications using Nano-QuIC would be beneficial. There are a host of RT-QuIC protocols that are already developed for CWD antemortem diagnostics that likely could seamlessly incorporate nanoparticle enhancement.<sup>51,52</sup> Additionally, antemortem RT-QuIC protocols have been developed for a large number of noninvasive sample types across a range of human diseases such as Parkinson's, Creutzfeldt-Jakob disease (CJD), etc.<sup>48,53,54</sup> While different substrate proteins are used for these tests, the fundamental principle of nanoparticle-aided amplification could potentially improve these assays for human disease diagnostics. Breakthroughs in traditional RT-QuIC protocols could also be readily employed in Nano-QuIC.

In conclusion, the ability of Nano-QuIC to overcome inhibitors, enhance diagnostic sensitivity and specificity, and reduce detection time collectively indicates the potential to significantly improve traditional RT-QuIC diagnostics. We note that variable results using siNPs might be observed when using protein substrates beyond the rHaPrP examined herein. It is possible that the siNP–rHaPrP interaction is specific to the protein template. Nevertheless, rHaPrP has emerged as an ideal substrate for a growing number of prion diagnostic protocols, including CJD, BSE, scrapie, and CWD. It is also possible that Nano-QuIC will require optimization for various biological and ecological samples. From a broader perspective, we believe that adaptations of Nano-QuIC will facilitate high-throughput diagnostic applications for a wide range of animal and human neurodegenerative diseases, paving the way for earlier detection and improved patient outcomes.

## ■ ASSOCIATED CONTENT

### Supporting Information

The Supporting Information is available free of charge at <https://pubs.acs.org/doi/10.1021/acs.nanolett.3c01001>.

Methods section summarizing tissue preparation, preparation of recombinant substrate, Nano-QuIC protocols, blinded sample set, and evaluation of kinetic data (PDF)

## ■ AUTHOR INFORMATION

### Corresponding Authors

**Peter A. Larsen** – Minnesota Center for Prion Research and Outreach (MNPRO) and Department of Veterinary and Biomedical Sciences, University of Minnesota, St. Paul, Minnesota 55108, United States; Email: [plarsen@umn.edu](mailto:plarsen@umn.edu)

**Sang-Hyun Oh** – Department of Electrical and Computer Engineering, University of Minnesota, Minneapolis, Minnesota 55455, United States; Minnesota Center for Prion Research and Outreach (MNPRO), University of Minnesota, St. Paul, Minnesota 55108, United States; [orcid.org/0000-0002-6992-5007](https://orcid.org/0000-0002-6992-5007); Email: [sang@umn.edu](mailto:sang@umn.edu)

### Authors

**Peter R. Christenson** – Department of Electrical and Computer Engineering, University of Minnesota, Minneapolis, Minnesota 55455, United States; Minnesota Center for Prion Research and Outreach (MNPRO), University of Minnesota, St. Paul, Minnesota 55108, United States; [orcid.org/0000-0003-3979-7945](https://orcid.org/0000-0003-3979-7945)

**Manci Li** – Minnesota Center for Prion Research and Outreach (MNPRO) and Department of Veterinary and Biomedical Sciences, University of Minnesota, St. Paul, Minnesota 55108, United States

**Gage Rowden** – Minnesota Center for Prion Research and Outreach (MNPRO) and Department of Veterinary and Biomedical Sciences, University of Minnesota, St. Paul, Minnesota 55108, United States

Complete contact information is available at: <https://pubs.acs.org/10.1021/acs.nanolett.3c01001>

## Author Contributions

S.-H.O. conceived the study. P.R.C. and G.R. performed molecular experiments. P.R.C., M.L., G.R., S.-H.O., and P.A.L. assisted with experimental design and interpreted the results. P.R.C., G.R., and M.L. performed statistical analyses. S.-H.O. and P.A.L. oversaw the research. All authors wrote and contributed to the final manuscript.

## Funding

Funding for research performed herein was provided by the Minnesota State Legislature through the Minnesota Legislative-Citizen Commission on Minnesota Resources (LCCMR) and Minnesota Agricultural Experiment Station Rapid Agricultural Response Fund to P.R.C., M.C., G.R., P.A.L., and S.-H.O., the Sanford P. Bordeau Chair in Electrical Engineering at the University of Minnesota and the McKnight Foundation to S.-H.O., and start-up funds awarded to P.A.L. through the Minnesota Agricultural, Research, Education, Extension and Technology Transfer (AGREETT) program. Portions of this work were conducted in the Minnesota Nano Center, which is supported by the National Science Foundation (NSF) through the National Nano Coordinated Infrastructure Network (NNCI) under Award ECCS-2025124. Portions of this work were carried out in the University of Minnesota Characterization Facility, which receives partial support from the NSF through the MRSEC (Award DMR-2011401) program.

## Notes

The authors declare no competing financial interest.

## ACKNOWLEDGMENTS

The authors thank the staff members of the NIH Rocky Mountain Laboratories, especially Byron Caughey, Andrew Hughson, and Christina Orrù, for training and assistance with the implementation of RT-QuIC and for supplying the original rPrP clone. Jason Bartz provided helpful comments on the manuscript. M. Schwabenlander provided valuable assistance in sample acquisition. S. Stone provided valuable logistical assistance with our molecular work. F. Schendel, T. Douville, and the staff of the University of Minnesota Biotechnology Resource Center provided critical support concerning the large-scale production of recombinant proteins. K. Wilson of the Colorado State University Veterinary Diagnostic Laboratory provided assistance with ELISA and IHC testing of samples reported herein. Some figures were created using BioRender ([BioRender.com](https://www.biorender.com)).

## REFERENCES

- (1) Prusiner, S. B. Nobel Lecture: Prions. *Proc. Natl. Acad. Sci. U.S.A.* **1998**, *95* (23), 13363–13383.
- (2) Soto, C.; Estrada, L. D. Protein Misfolding and Neurodegeneration. *Arch. Neurol.* **2008**, *65* (2), 184–189.
- (3) Marsh, R. F.; Kincaid, A. E.; Bessen, R. A.; Bartz, J. C. Interspecies Transmission of Chronic Wasting Disease Prions to Squirrel Monkeys (*Saimiri Sciureus*). *J. Virol.* **2005**, *79* (21), 13794–13796.
- (4) Kim, Y.; Park, J.-H.; Lee, H.; Nam, J.-M. How Do the Size, Charge and Shape of Nanoparticles Affect Amyloid  $\beta$  Aggregation on Brain Lipid Bilayer? *Sci. Rep.* **2016**, *6*, 19548.
- (5) Irazo, A.; Fairfoul, G.; Ayudhaya, A. C. N.; Serradell, M.; Gelpi, E.; Vilaseca, I.; Sanchez-Valle, R.; Gaig, C.; Santamaria, J.; Tolosa, E.; Riha, R. L.; Green, A. J. E. Detection of  $\alpha$ -Synuclein in CSF by RT-QuIC in Patients with Isolated Rapid-Eye-Movement Sleep Behaviour Disorder: A Longitudinal Observational Study. *Lancet Neurol* **2021**, *20* (3), 203–212.

- (6) Dong, T.-T.-T.; Satoh, K. The Latest Research on RT-QuIC Assays-A Literature Review. *Pathogens* **2021**, *10* (3), 305.
- (7) Davenport, K. A.; Hoover, C. E.; Denkers, N. D.; Mathiason, C. K.; Hoover, E. A. Modified Protein Misfolding Cyclic Amplification Overcomes Real-Time Quaking-Induced Conversion Assay Inhibitors in Deer Saliva To Detect Chronic Wasting Disease Prions. *J. Clin. Microbiol.* **2018**, *56* (9), e00947–18.
- (8) Mead, S.; Khalili-Shirazi, A.; Potter, C.; Mok, T.; Nihat, A.; Hyare, H.; Canning, S.; Schmidt, C.; Campbell, T.; Darwent, L.; Muirhead, N.; Ebsworth, N.; Hextall, P.; Wakeling, M.; Linehan, J.; Libri, V.; Williams, B.; Jaunmuktane, Z.; Brandner, S.; Rudge, P.; Collinge, J. Prion Protein Monoclonal Antibody (PRN100) Therapy for Creutzfeldt–Jakob Disease: Evaluation of a First-in-Human Treatment Programme. *Lancet Neurol* **2022**, *21* (4), 342–354.
- (9) Haley, N. J.; Richt, J. A. Evolution of Diagnostic Tests for Chronic Wasting Disease, a Naturally Occurring Prion Disease of Cervids. *Pathogens* **2017**, *6* (3), 35.
- (10) Parnetti, L.; Gaetani, L.; Eusebi, P.; Paciotti, S.; Hansson, O.; El-Agnaf, O.; Mollenhauer, B.; Blennow, K.; Calabresi, P. CSF and Blood Biomarkers for Parkinson's Disease. *Lancet Neurol* **2019**, *18* (6), 573–586.
- (11) Haley, N. J.; Mathiason, C. K.; Carver, S.; Telling, G. C.; Zabel, M. D.; Hoover, E. A. Sensitivity of Protein Misfolding Cyclic Amplification versus Immunohistochemistry in Ante-Mortem Detection of Chronic Wasting Disease. *J. Gen. Virol.* **2012**, *93*, 1141–1150.
- (12) Coysh, T.; Mead, S. The Future of Seed Amplification Assays and Clinical Trials. *Front. Aging Neurosci.* **2022**, *14*, 872629.
- (13) Telling, G. C. Breakthroughs in Antemortem Diagnosis of Neurodegenerative Diseases. *Proc. Natl. Acad. Sci. U.S.A.* **2019**, *116* (46), 22894–22896.
- (14) Schwabenlander, M. D.; Rowden, G. R.; Li, M.; LaSharr, K.; Hildebrand, E. C.; Stone, S.; Seelig, D. M.; Jennelle, C. S.; Cornicelli, L.; Wolf, T. M.; et al. Comparison of Chronic Wasting Disease Detection Methods and Procedures: Implications for Free-Ranging White-Tailed Deer (*Odocoileus virginianus*) Surveillance and Management. *J. Wildl. Dis.* **2022**, *58*, 50–62.
- (15) Li, M.; Schwabenlander, M. D.; Rowden, G. R.; Schefers, J. M.; Jennelle, C. S.; Carstensen, M.; Seelig, D.; Larsen, P. A. RT-QuIC Detection of CWD Prion Seeding Activity in White-Tailed Deer Muscle Tissues. *Sci. Rep.* **2021**, *11*, 16759.
- (16) Orrù, C. D.; Isiofia, O.; Hughson, A. G.; Caughey, B. Real-Time Quaking-Induced Conversion (QuIC) Assays for the Detection and Diagnosis of Human Prion Diseases. In *Prions and Diseases*; Zou, W.-Q., Gambetti, P., Eds.; Springer International Publishing: Cham, Switzerland, 2023; pp 621–635.
- (17) Nonno, R.; Di Bari, M. A.; Pirisinu, L.; D'Agostino, C.; Vanni, I.; Chiappini, B.; Marcon, S.; Riccardi, G.; Tran, L.; Vikøren, T.; Våge, J.; Madslie, K.; Mitchell, G.; Telling, G. C.; Benestad, S. L.; Agrimi, U. Studies in Bank Voles Reveal Strain Differences between Chronic Wasting Disease Prions from Norway and North America. *Proc. Natl. Acad. Sci. U.S.A.* **2020**, *117* (49), 31417–31426.
- (18) Tranulis, M. A.; Gavier-Widén, D.; Våge, J.; Nöremark, M.; Korpenfelt, S.-L.; Hautaniemi, M.; Pirisinu, L.; Nonno, R.; Benestad, S. L. Chronic Wasting Disease in Europe: New Strains on the Horizon. *Acta Vet. Scand.* **2021**, *63* (1), 48.
- (19) Otero, A.; Velásquez, C. D.; Aiken, J.; McKenzie, D. Chronic Wasting Disease: A Cervid Prion Infection Looming to Spillover. *Vet. Res.* **2021**, *52* (1), 115.
- (20) Yuan, Q.; Rowden, G.; Wolf, T. M.; Schwabenlander, M. D.; Larsen, P. A.; Bartelt-Hunt, S. L.; Bartz, J. C. Sensitive Detection of Chronic Wasting Disease Prions Recovered from Environmentally Relevant Surfaces. *Environ. Int.* **2022**, *166*, 107347.
- (21) Hannaoui, S.; Zemlyankina, I.; Chang, S. C.; Arifin, M. I.; Béringue, V.; McKenzie, D.; Schatzl, H. M.; Gilch, S. Transmission of Cervid Prions to Humanized Mice Demonstrates the Zoonotic Potential of CWD. *Acta Neuropathol* **2022**, *144* (4), 767–784.
- (22) Denkers, N. D.; Henderson, D. M.; Mathiason, C. K.; Hoover, E. A. Enhanced Prion Detection in Biological Samples by Magnetic

- Particle Extraction and Real-Time Quaking-Induced Conversion. *J. Gen. Virol.* **2016**, *97* (8), 2023–2029.
- (23) Sepúlveda, B.; Angelomé, P. C.; Lechuga, L. M.; Liz-Marzán, L. M. LSPR-Based Nanobiosensors. *Nano Today* **2009**, *4* (3), 244–251.
- (24) Belushkin, A.; Yesilkoy, F.; Altug, H. Nanoparticle-Enhanced Plasmonic Biosensor for Digital Biomarker Detection in a Microarray. *ACS Nano* **2018**, *12* (5), 4453–4461.
- (25) Akkilic, N.; Geschwindner, S.; Höök, F. Single-Molecule Biosensors: Recent Advances and Applications. *Biosens. Bioelectron.* **2020**, *151*, 111944.
- (26) Christenson, P. R.; Li, M.; Rowden, G.; Schwabenlander, M. D.; Wolf, T. M.; Oh, S.-H.; Larsen, P. A. A Field-Deployable Diagnostic Assay for the Visual Detection of Misfolded Prions. *Sci. Rep.* **2022**, *12*, 12246.
- (27) Kumar, A.; Kim, S.; Nam, J.-M. Plasmonically Engineered Nanoprobes for Biomedical Applications. *J. Am. Chem. Soc.* **2016**, *138* (44), 14509–14525.
- (28) Jackman, J. A.; Rahim Ferhan, A.; Cho, N.-J. Nanoplasmonic Sensors for Biointerfacial Science. *Chem. Soc. Rev.* **2017**, *46* (12), 3615–3660.
- (29) Grigolato, F.; Colombo, C.; Ferrari, R.; Rezabkova, L.; Arosio, P. Mechanistic Origin of the Combined Effect of Surfaces and Mechanical Agitation on Amyloid Formation. *ACS Nano* **2017**, *11* (11), 11358–11367.
- (30) Tahaei Gilan, S. S.; Yahya Rayat, D.; Ahmed Mustafa, T.; Aziz, F. M.; Shahpasand, K.; Akhtari, K.; Salihi, A.; Abou-Zied, O. K.; Falahati, M.  $\alpha$ -Synuclein Interaction with Zero-Valent Iron Nanoparticles Accelerates Structural Rearrangement into Amyloid-Susceptible Structure with Increased Cytotoxic Tendency. *Int. J. Nanomedicine* **2019**, *14*, 4637–4648.
- (31) Konar, M.; Mathew, A.; Dasgupta, S. Effect of Silica Nanoparticles on the Amyloid Fibrillation of Lysozyme. *ACS Omega* **2019**, *4* (1), 1015–1026.
- (32) Zhou, S.; Zhu, Y.; Yao, X.; Liu, H. Carbon Nanoparticles Inhibit the Aggregation of Prion Protein as Revealed by Experiments and Atomistic Simulations. *J. Chem. Inf. Model.* **2019**, *59* (5), 1909–1918.
- (33) Mohammadi, S.; Nikkhah, M.  $\text{TiO}_2$  Nanoparticles as Potential Promoting Agents of Fibrillation of  $\alpha$ -Synuclein, a Parkinson's Disease-Related Protein. *Iran. J. Biotechnol.* **2017**, *15* (2), 87–94.
- (34) Gladysz, A.; Wagner, M.; Häupl, T.; Elsner, C.; Abel, B. Structure-Making Effects of Metal Nanoparticles in Amyloid Peptide Fibrillation. *Part. Part. Syst. Charact.* **2015**, *32* (5), 573–582.
- (35) Linse, S.; Cabaleiro-Lago, C.; Xue, W.-F.; Lynch, I.; Lindman, S.; Thulin, E.; Radford, S. E.; Dawson, K. A. Nucleation of Protein Fibrillation by Nanoparticles. *Proc. Natl. Acad. Sci. U.S.A.* **2007**, *104* (21), 8691–8696.
- (36) Cabaleiro-Lago, C.; Szczepankiewicz, O.; Linse, S. The Effect of Nanoparticles on Amyloid Aggregation Depends on the Protein Stability and Intrinsic Aggregation Rate. *Langmuir* **2012**, *28* (3), 1852–1857.
- (37) Grigolato, F.; Arosio, P. The Role of Surfaces on Amyloid Formation. *Biophys. Chem.* **2021**, *270*, 106533.
- (38) Zhang, D.; Neumann, O.; Wang, H.; Yuwono, V. M.; Barhouni, A.; Perham, M.; Hartgerink, J. D.; Wittung-Stafshede, P.; Halas, N. J. Gold Nanoparticles Can Induce the Formation of Protein-Based Aggregates at Physiological pH. *Nano Lett.* **2009**, *9* (2), 666–671.
- (39) Orrù, C. D.; Hughson, A. G.; Groveman, B. R.; Campbell, K. J.; Anson, K. J.; Manca, M.; Kraus, A.; Caughey, B. Factors That Improve RT-QuIC Detection of Prion Seeding Activity. *Viruses* **2016**, *8* (5), 140.
- (40) Nielsen, L.; Khurana, R.; Coats, A.; Frokjaer, S.; Brange, J.; Vyas, S.; Uversky, V. N.; Fink, A. L. Effect of Environmental Factors on the Kinetics of Insulin Fibril Formation: Elucidation of the Molecular Mechanism. *Biochemistry* **2001**, *40* (20), 6036–6046.
- (41) Uversky, V. N.; Li, J.; Fink, A. L. Evidence for a Partially Folded Intermediate in  $\alpha$ -Synuclein Fibril Formation. *J. Biol. Chem.* **2001**, *276* (14), 10737–10744.
- (42) John, T.; Gladysz, A.; Kubeil, C.; Martin, L. L.; Risselada, H. J.; Abel, B. Impact of Nanoparticles on Amyloid Peptide and Protein Aggregation: A Review with a Focus on Gold Nanoparticles. *Nanoscale* **2018**, *10* (45), 20894–20913.
- (43) Alvarez, Y. D.; Fauerbach, J. A.; Pellegrotti, J. V.; Jovin, T. M.; Jares-Erijman, E. A.; Stefani, F. D. Influence of Gold Nanoparticles on the Kinetics of  $\alpha$ -Synuclein Aggregation. *Nano Lett.* **2013**, *13* (12), 6156–6163.
- (44) Eraña, H.; Pérez-Castro, M. Á.; García-Martínez, S.; Charco, J. M.; López-Moreno, R.; Díaz-Domínguez, C. M.; Barrio, T.; González-Miranda, E.; Castilla, J. A Novel, Reliable and Highly Versatile Method to Evaluate Different Prion Decontamination Procedures. *Front Bioeng Biotechnol* **2020**, *8*, 589182.
- (45) Masson, J.-F. Surface Plasmon Resonance Clinical Biosensors for Medical Diagnostics. *ACS Sens* **2017**, *2* (1), 16–30.
- (46) Surguchov, A. Analysis of Protein Conformational Strains-A Key for New Diagnostic Methods of Human Diseases. *Int. J. Mol. Sci.* **2020**, *21* (8), 2801.
- (47) Groveman, B. R.; Orrù, C. D.; Hughson, A. G.; Raymond, L. D.; Zanusso, G.; Ghetti, B.; Campbell, K. J.; Safar, J.; Galasko, D.; Caughey, B. Rapid and Ultra-Sensitive Quantitation of Disease-Associated  $\alpha$ -Synuclein Seeds in Brain and Cerebrospinal Fluid by  $\alpha$ Syn RT-QuIC. *Acta Neuropathol Commun.* **2018**, *6* (1), 7.
- (48) Manne, S.; Kondru, N.; Jin, H.; Serrano, G. E.; Anantharam, V.; Kanthasamy, A.; Adler, C. H.; Beach, T. G.; Kanthasamy, A. G. Blinded RT-QuIC Analysis of  $\alpha$ -Synuclein Biomarker in Skin Tissue From Parkinson's Disease Patients. *Mov. Disord.* **2020**, *35* (12), 2230–2239.
- (49) De Luca, C. M. G.; Elia, A. E.; Portaleone, S. M.; Cazzaniga, F. A.; Rossi, M.; Bistaffa, E.; De Cecco, E.; Narkiewicz, J.; Salzano, G.; Carletta, O.; et al. Efficient RT-QuIC Seeding Activity for  $\alpha$ -Synuclein in Olfactory Mucosa Samples of Patients with Parkinson's Disease and Multiple System Atrophy. *Transl. Neurodegener.* **2019**, *8*, 24.
- (50) Fairfoul, G.; McGuire, L. I.; Pal, S.; Ironside, J. W.; Neumann, J.; Christie, S.; Joachim, C.; Esiri, M.; Evetts, S. G.; Rolinski, M.; Baig, F.; Ruffmann, C.; Wade-Martins, R.; Hu, M. T. M.; Parkkinen, L.; Green, A. J. E. Alpha-Synuclein RT-QuIC in the CSF of Patients with Alpha-Synucleinopathies. *Ann. Clin. Transl. Neurol.* **2016**, *3* (10), 812–818.
- (51) Tennant, J. M.; Li, M.; Henderson, D. M.; Tyer, M. L.; Denkers, N. D.; Haley, N. J.; Mathiason, C. K.; Hoover, E. A. Shedding and Stability of CWD Prion Seeding Activity in Cervid Feces. *PLoS One* **2020**, *15* (3), No. e0227094.
- (52) Ferreira, N. C.; Charco, J. M.; Plagenz, J.; Orrù, C. D.; Denkers, N. D.; Metrick, M. A., 2nd; Hughson, A. G.; Griffin, K. A.; Race, B.; Hoover, E. A.; et al. Detection of Chronic Wasting Disease in Mule and White-Tailed Deer by RT-QuIC Analysis of Outer Ear. *Sci. Rep.* **2021**, *11*, 7702.
- (53) Poggiolini, I.; Gupta, V.; Lawton, M.; Lee, S.; El-Turabi, A.; Querejeta-Coma, A.; Trenkwalder, C.; Sixel-Döring, F.; Foubert-Samier, A.; Pavy-Le Traon, A.; Plazzi, G.; Biscarini, F.; Montplaisir, J.; Gagnon, J.-F.; Postuma, R. B.; Antelmi, E.; Meissner, W. G.; Mollenhauer, B.; Ben-Shlomo, Y.; Hu, M. T.; Parkkinen, L. Diagnostic Value of Cerebrospinal Fluid Alpha-Synuclein Seed Quantification in Synucleinopathies. *Brain* **2022**, *145* (2), 584–595.
- (54) Orrù, C. D.; Groveman, B. R.; Hughson, A. G.; Zanusso, G.; Coulthart, M. B.; Caughey, B. Rapid and Sensitive RT-QuIC Detection of Human Creutzfeldt-Jakob Disease Using Cerebrospinal Fluid. *MBio* **2015**, *6* (1), e02451–14.



## OPEN Ticks harbor and excrete chronic wasting disease prions

H. N. Inzalaco<sup>1✉</sup>, F. Bravo-Risi<sup>2,3</sup>, R. Morales<sup>2,3</sup>, D. P. Walsh<sup>4</sup>, D. J. Storm<sup>5</sup>, J. A. Pedersen<sup>6,9</sup>, W. C. Turner<sup>7</sup> & S. S. Lichtenberg<sup>8</sup>

Chronic wasting disease (CWD) is a fatal neurodegenerative disease caused by infectious prions (PrP<sup>CWD</sup>) affecting cervids. Circulating PrP<sup>CWD</sup> in blood may pose a risk for indirect transmission by way of hematophagous ectoparasites acting as mechanical vectors. Cervids can carry high tick infestations and exhibit allogrooming, a common tick defense strategy between conspecifics. Ingestion of ticks during allogrooming may expose naïve animals to CWD, if ticks harbor PrP<sup>CWD</sup>. This study investigates whether ticks can harbor transmission-relevant quantities of PrP<sup>CWD</sup> by combining experimental tick feeding trials and evaluation of ticks from free-ranging white-tailed deer (*Odocoileus virginianus*). Using the real-time quaking-induced conversion (RT-QuIC) assay, we show that black-legged ticks (*Ixodes scapularis*) fed PrP<sup>CWD</sup>-spiked blood using artificial membranes ingest and excrete PrP<sup>CWD</sup>. Combining results of RT-QuIC and protein misfolding cyclic amplification, we detected seeding activity from 6 of 15 (40%) pooled tick samples collected from wild CWD-infected white-tailed deer. Seeding activities in ticks were analogous to 10–1000 ng of CWD-positive retroparyngeal lymph node collected from deer upon which they were feeding. Estimates revealed a median infectious dose range of 0.3–42.4 per tick, suggesting that ticks can take up transmission-relevant amounts of PrP<sup>CWD</sup> and may pose a CWD risk to cervids.

Chronic wasting disease (CWD) is an infectious, slowly progressing, and invariably fatal neurodegenerative disease afflicting wild and domestic cervids. Both direct and indirect routes of exposure and transmission have contributed to endemic increases and broad geographic spread of CWD<sup>1</sup>. However, there are significant gaps in our understanding of how CWD is transmitted among susceptible hosts. Proposed putative routes of exposure and transmission among susceptible cervid species include sexual contact<sup>2</sup>, consumption of contaminated soil, water, and plants<sup>3–5</sup>, mucosal contact with contaminated fomites<sup>6</sup>, or antler cannibalism behavior<sup>7</sup>. With many unknowns about transmission pathways and their relative risks it is prudent to consider how host behavior and life-history traits facilitate CWD exposure events. Here we examine the potential for ticks to contribute to indirect transmission of CWD.

In the host, CWD presents with a broad distribution of disease-associated prions (PrP<sup>CWD</sup>) in peripheral tissues and biological fluids prior to neuroinvasion. Blood of prion-infected animals harbors infectivity at the pre-symptomatic disease stage with relatively higher circulating amounts of PrP<sup>CWD</sup> than those found in urine<sup>8</sup> or feces<sup>9</sup>. Animal challenge studies demonstrate that CWD-positive whole blood has a disease attack rate of up to 100% in cervids following intravenous exposure with 250 mL and 22% in cervidized mice following oral exposure with 150 µL<sup>10</sup>.

Arthropods that interact with cervids, such as biting flies or blood-obligate ectoparasites, could play a role in prion transmission. Early investigations revealed that homogenates of several species of mites gathered from scrapie infected sheep farms harbored infectivity following intracerebral (i.c.) and intraperitoneal (i.p.) exposure of mice<sup>11</sup>. Recent studies examining the role of ticks in transmission of transmissible spongiform encephalopathies (TSEs) suggest that nymphal ticks would be poor mechanical vectors for certain disease-causing prions, but that adults of at least one species of Ixodid tick may have the potential to take up PrP<sup>CWD</sup><sup>12,13</sup>. Ticks possess several biological and behavioral traits that may implicate their involvement in indirect transmission. Ticks take a blood

<sup>1</sup>Wisconsin Cooperative Wildlife Research Unit, Department of Forest and Wildlife Ecology, University of Wisconsin, Madison, Madison, WI 53706, USA. <sup>2</sup>Department of Neurology, The University of Texas Health Science Center at Houston, Houston, TX, USA. <sup>3</sup>Centro Integrativo de Biología y Química Aplicada (CIBQA), Universidad Bernardo O'Higgins, Santiago, Chile. <sup>4</sup>U.S. Geological Survey, Montana Cooperative Wildlife Research Unit, University of Montana, Missoula, MT, USA. <sup>5</sup>Wisconsin Department of Natural Resources, Eau Claire, WI, USA. <sup>6</sup>Environmental Health and Engineering, Johns Hopkins University, Baltimore, MD 21218, USA. <sup>7</sup>Wisconsin Cooperative Wildlife Research Unit, Department of Forest and Wildlife Ecology, U.S. Geological Survey, University of Wisconsin – Madison, Madison, WI 53706, USA. <sup>8</sup>Department of Soil Science, University of Wisconsin, Madison, Madison, WI, USA. <sup>9</sup>J. A. Pedersen is deceased. ✉email: inzalaco@wisc.edu

meal that can range in volume from 0.3 mL to as high as 8.9 mL per female<sup>14</sup>. Ixodid ticks remain attached to one bite location for as long as 14 days<sup>14</sup>, during which time there is a rapid engorgement phase in the last 24–36 h where consumed blood is concentrated due to reduced digestion and excretion of water and electrolytes<sup>15</sup>. This concentration of blood meal results in a fed body weight increase in excess of 100 times their unfed weight<sup>16</sup>. This tick feeding behavior may be pertinent to disease transmission since it may concentrate infectious prions.

Arthropods and other invertebrates do not express cellular prion (PrP<sup>C</sup>), a prerequisite for establishing a prion infection<sup>17</sup>, indicating that a more likely role for prion disease transmission by ticks would be as a mechanical vector rather than as a biological vector. Cervids may encounter ticks harboring prion infected blood during bouts of allogrooming, an ectoparasite-defense strategy used by social mammals<sup>18</sup> that involves grooming between members of the same species. This form of grooming is one of the most common nonaggressive interactions among females, females and young, as well as among males during the non-mating season of several cervid species<sup>18,19</sup>. Higher ectoparasite infestations increase allogrooming behavior in cervids such as white-tailed deer (*Odocoileus virginianus*, WTD)<sup>19</sup> and elk (*Cervus canadensis*)<sup>18</sup>, during which ectoparasites may be consumed intentionally or unintentionally, as a result of grooming mechanics such as licking, or nibbling and chewing<sup>19</sup>. These host and parasite traits may make allogrooming a possible transmission pathway for CWD, if hosts consume partially or fully engorged ticks during bouts of allogrooming.

Using an ultrasensitive in vitro protein amplification assay, real-time quaking-induced conversion (RT-QuIC), we investigate this hypothesized pathway to (i) determine experimentally if ticks can harbor prions taken up from infected blood meals and (ii) survey ticks on CWD-positive WTD to determine if PrP<sup>CWD</sup> can be detected in ticks collected from free-ranging deer in a CWD endemic region. Given that prion seeding activity was detected in these ticks, we further (iii) estimated amounts of PrP<sup>CWD</sup> found in ticks relative to amounts of PrP<sup>CWD</sup> found in CWD-positive deer lymphatic tissues, and (iv) estimated a per-tick infectious dose (ID<sub>50</sub>) based on the pooled tick amyloid formation rate (AFR) (i.e., 1/time to threshold) equivalence to AFRs of retropharyngeal lymph node (RPLN) combined with an established minimum mass of CWD-positive brain sufficient to orally transmit CWD.

## Results

Our experimental spiking studies aimed to test recovery of PrP<sup>CWD</sup> from different sample types, using a brain sample (from the obex region) from a late-stage CWD-positive WTD as the source material for spiking in all experiments. We were able to detect PrP<sup>CWD</sup> using RT-QuIC from samples spiked with PrP<sup>CWD</sup>, including blood, tick homogenates and homogenates of ticks fed blood spiked with PrP<sup>CWD</sup>. Whole blood or tick homogenates spiked with tenfold dilutions of CWD-positive brain homogenates showed sensitivity of at least 10<sup>-6</sup>, which corresponds with the sensitivity detection limit for the brain sample used for the spiking experiments (Fig. 1a,b,c,d). Blood and engorged tick homogenates spiked with 10<sup>-3</sup> through 10<sup>-5</sup> dilutions of CWD-positive brain showed PrP<sup>CWD</sup> seeding activity (assay fluorescence from sample with PrP<sup>CWD</sup> present) in 8/8 technical replicates (Fig. 1a,b,c). The blood and tick homogenates spiked with the 10<sup>-6</sup> dilution of the CWD-positive brain showed PrP<sup>CWD</sup> seeding activity in 7/8 and 4/8 replicates, respectively (Fig. 1a,b,c). Neither blood nor tick homogenate sample types produced any false seeding activity, constituting a specificity rate of 100% for each sample type using the RT-QuIC assay in these spiking experiments (Fig. 1a). AFR values for brain-spiked samples differed among sample types ( $F(2, 68) = 18.626, p < 0.0001$ ), with mean AFR values higher for blood (mean  $\pm$  standard error:  $0.1 \pm 0.003$ ), compared with brain ( $0.09 \pm 0.004$ ), or tick homogenates ( $0.08 \pm 0.003$ ; Tukey honestly significant difference (HSD) post-hoc test blood versus brain:  $0.01 \pm 0.006, p = 0.03$ ; blood versus tick:  $0.2 \pm 0.005, p < 0.001$ ). AFR values for all sample types decreased across the dilution series ( $F(3, 68) = 131.352, p < 0.0001$ ), however, there was no statistically significant interaction between AFR values by sample type across the dilution series ( $F(6, 68) = 0.871, p > 0.05$ ).

To evaluate whether ticks can take up and excrete prions, we used a previously established artificial tick membrane-feeding system<sup>20</sup> to feed *I. scapularis* a blood meal inoculated with a 10<sup>-3</sup> dilution of CWD-positive brain (10<sup>6</sup> ng) (Fig. 1e,f,g). Although, the relative amounts of PrP<sup>CWD</sup> found in blood of CWD-infected deer is likely ~ 1000-fold less than the dilution used to inoculate blood meals<sup>21</sup>, this 10<sup>-3</sup> mg/mL dilution was chosen to demonstrate the potential for *I. scapularis* to assimilate prions from a blood meal rather than demonstrate natural uptake. Feeding assay attachment rates reached 100% by 72 h following placement of adult female and male ticks within blood-exposed feeding chambers for all treatment groups and individual engorgement occurred between day 9 and 14 across both treatment groups. Serial dilutions of tick homogenates from the 10<sup>-3</sup> PrP<sup>CWD</sup> membrane-fed exposure group demonstrated PrP<sup>CWD</sup> seeding activity in 15/24, 24/24, 15/24, and 2/24 technical replicates for inoculum-based dilutions of 10<sup>-3</sup> through 10<sup>-6</sup>, respectively (Fig. 1h,j). Serial dilutions of tick frass collected from the 10<sup>-3</sup> PrP<sup>CWD</sup> treatment group demonstrated seeding activity in 24/24 replicates for inoculum-based dilutions of 10<sup>-3</sup> through 10<sup>-5</sup>, and 22/24 replicates for the 10<sup>-6</sup> inoculum-based dilution (Fig. 1h,i). AFR values were significantly different based on sample type ( $F(2, 196) = 24.753, p < 0.0001$ ). Mean AFRs were significantly higher for frass (mean  $\pm$  standard error:  $0.093 \pm 0.0038$ ), and brain ( $0.088 \pm 0.0094$ ), compared to tick homogenates ( $0.06 \pm 0.004$ ; Tukey HSD post-hoc test of frass versus tick:  $0.04, \pm 0.005, p < 0.0001$ ; brain versus tick:  $0.03, \pm 0.010, p = 0.005$ ). AFR values differed along the dilution series ( $F(3, 196) = 24.848, p < 0.0001$ ), with a significant interaction between sample type and dilution ( $F(6, 196) = 5.759, p < 0.0001$ ; significant Tukey HSD post-hoc test: frass and brain for the 10<sup>-3</sup> dilution:  $-0.05, \pm 0.02, p = 0.036$ ; frass and tick at dilutions 10<sup>-4</sup> to 10<sup>-6</sup>:  $+0.05, \pm 0.01, p < 0.0001$ ;  $0.07, \pm 0.01, p < 0.0001$ ;  $0.05, \pm 0.01, p < 0.0001$ , respectively).

After these proof-of-concept experiments, we examined ~ 2000 Wisconsin hunter-harvested deer heads for ticks. Of the 2000 heads examined, 174 were tick-infested. From the sample set of 174 heads infested with ticks that were evaluated for CWD in RPLN through enzyme-linked immunosorbent assay (ELISA), 15 tested positive (data not shown). CWD status in these heads were cross-confirmed by RT-QuIC, providing similar results. Then, we determined if prions could be detected in ear tissue and in engorged ticks from these 15 CWD-positive

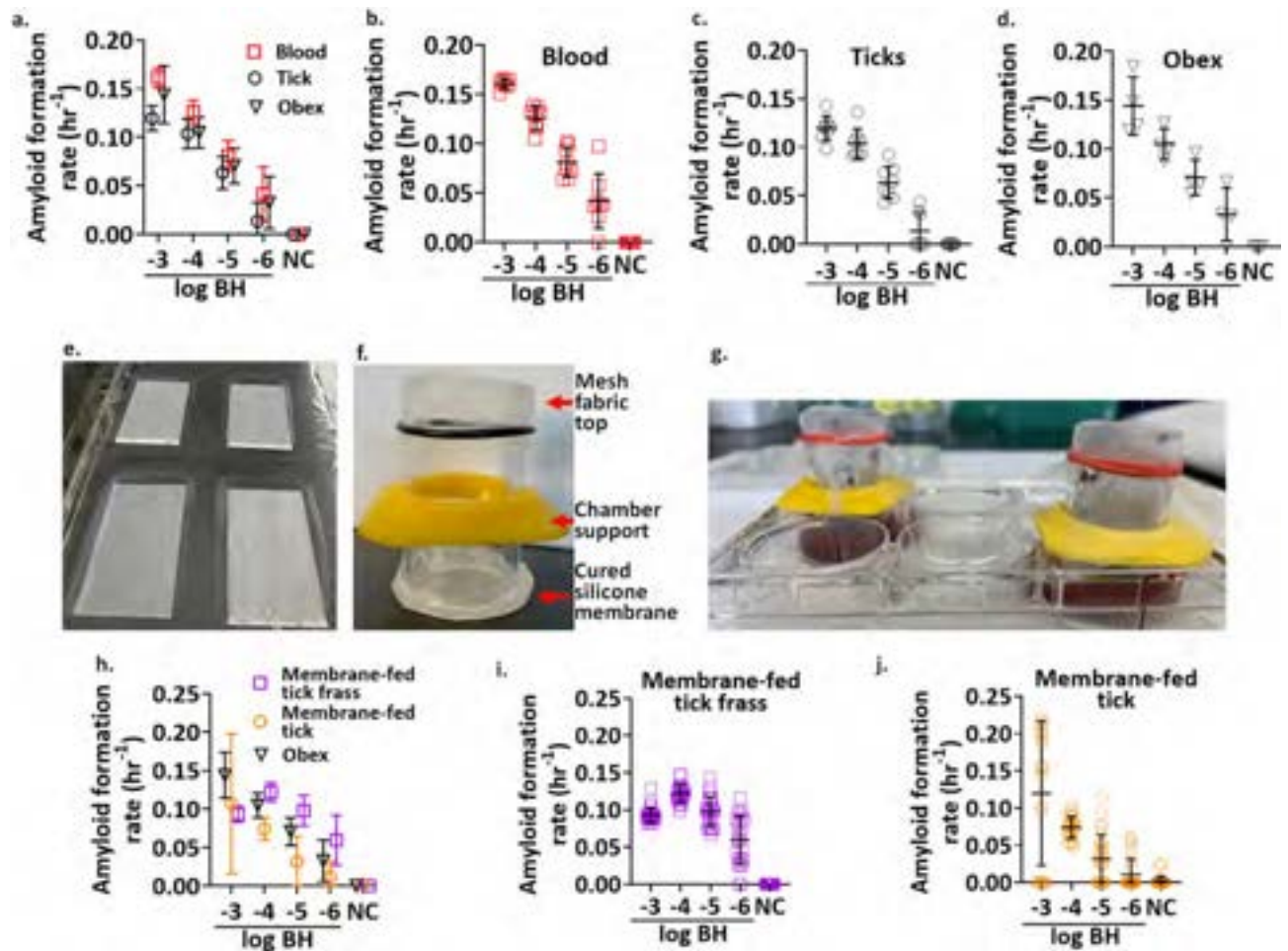


**Figure 1.** Recovery of chronic wasting disease (CWD) prions ( $\text{PrP}^{\text{CWD}}$ ) from spiking and membrane feeding experiments for analysis using the real-time quaking-induced conversion (RT-QuIC) assay. Comparison of amyloid formation rates (AFR) by RT-QuIC of (a–c) defibrinated bovine whole blood spiked with a  $10^{-3}$  dilution of the same 10% brain homogenate as used for the brain dilution series, and artificial membrane-fed tick homogenates spiked in the same manner as the blood (“b” and “c” depict AFRs of all 8 technical replicates for spiked whole blood or tick homogenates averaged in “a”) or (d) tenfold dilutions of 10% brain homogenate (BH) (from the obex region) from a CWD-positive white-tailed deer. Membrane feeding units were constructed using (e) cured silicon membranes adhered to the base of (f) assembled feeding chambers. (g) Depiction of the assembled feeding unit with feeding chambers being held upright by the chamber supports. (h–j) Comparison of AFRs by RT-QuIC of homogenates from membrane-fed  $\text{PrP}^{\text{CWD}}$  exposed or negative control ticks and tick frass (“i” and “j” depict AFRs for all 24 technical replicates (from 3 biological replicates run on 3 separate plates) for frass or membrane-fed tick homogenates averaged in “h”). Negative controls (NC) in each AFR plot are representative for the same sample type.

WTD (See Supplementary Table S1 for county harvested in). As negative control, 15 additional pooled tick samples collected from CWD-negative WTD were included in this analysis but were analyzed without blinding in completely separate experiments (Supplemental Figures S1 and S2). The number of attached and partially or fully engorged ticks collected from each WTD head examined, regardless of CWD status, ranged from 1 to 30 ( $6.1 \pm 5.4$ ). The number of attached ticks ranged from 2 to 8 ( $3.7 \pm 1.8$ ) for the 15 CWD-positive deer heads and 3 to 16 ( $5.3 \pm 4.4$ ) for the 15 CWD-negative deer heads.

No false seeding activity was observed for tick or ear tissue samples collected from CWD-negative WTD. However, detection of  $\text{PrP}^{\text{CWD}}$  in these peripheral samples (ticks and ear tissue) was limited compared to detection in RPLN for each of the 15 CWD-positive WTD (Fig. 2a, Supplementary Table S2). Comparing AFR values among sample types, ear samples were positively correlated with wild-fed tick samples ( $R^2 = 0.5$ ,  $t = 3.62$ ,  $p$ -value = 0.003,  $N = 15$ ; Fig. 2d), suggesting that ticks may perform as well as ear tissues in detecting prions. However, RPLN AFRs were not correlated with seeding activity in either ear tissues ( $R^2 = 0.15$ ,  $t = 1.51$ ,  $p$ -value = 0.155,  $N = 15$ ; Fig. 2c) or tick samples ( $R^2 = 0.02$ ,  $t = 0.5$ ,  $p$ -value = 0.628,  $N = 15$ ; Fig. 2e), indicating that these peripheral samples had reduced sensitivity for detecting prions compared to the RPLN tissue samples in our study using RT-QuIC. Most of the ear samples showed positive seeding activity to only a  $10^{-2}$  dilution using RT-QuIC, however those that demonstrated seeding activity out to a  $10^{-3}$ ,  $10^{-4}$ ,  $10^{-5}$  dilution also appeared to be reflective

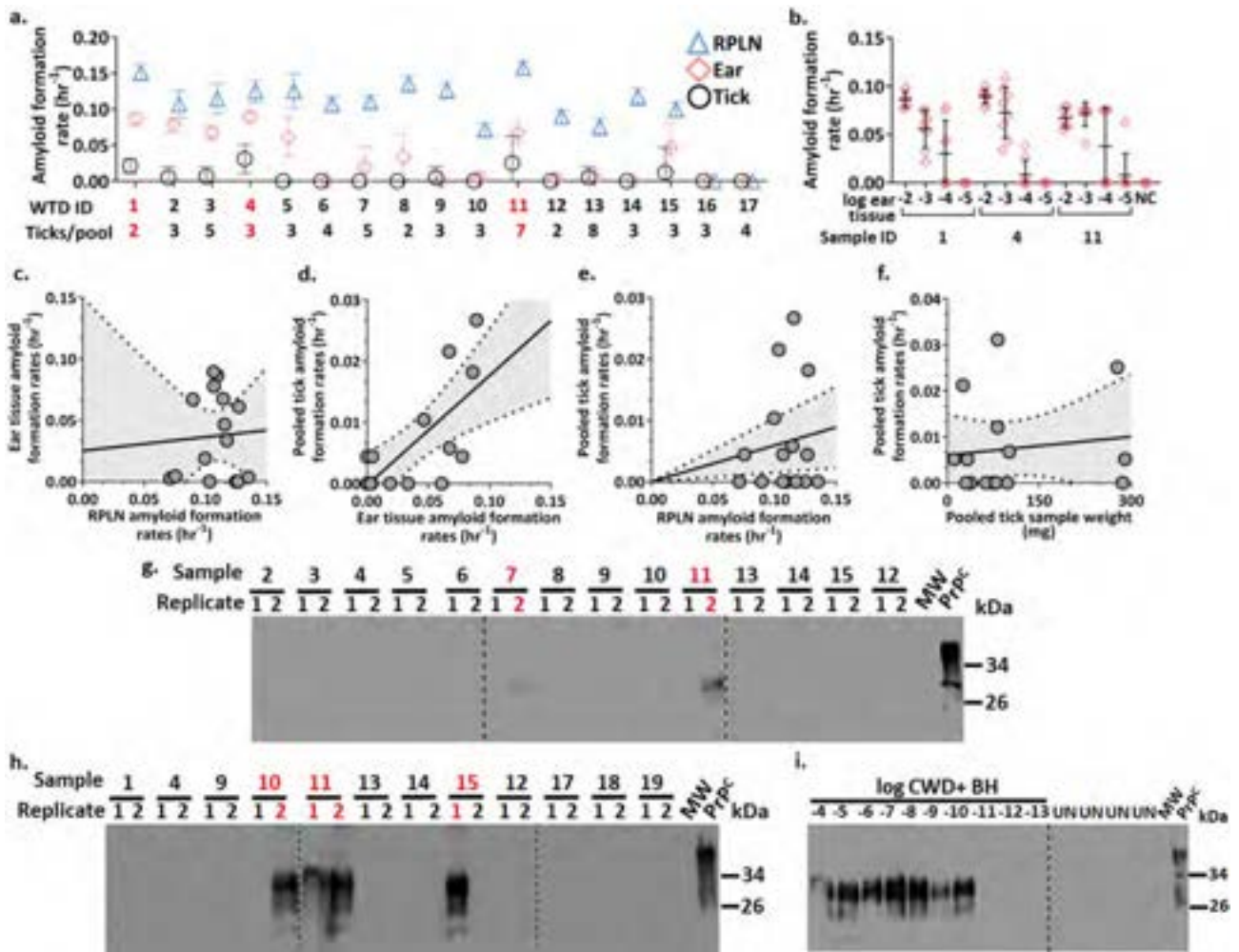


**Figure 2.** Presence of chronic wasting disease (CWD) prions (PrP<sup>CWD</sup>) in tissues and *Ixodes scapularis* from hunter-harvested white-tailed deer (WTD) assessed by two protein amplification assays. Comparisons of real-time quaking-induced conversion (RT-QuIC) amyloid formation rates (AFR) for (a) deer retropharyngeal lymph node (RPLN), ear tissue (pinna), and pooled tick samples from 15 CWD-positive (ID 1–15) and two of the 15 CWD-negative (ID 16,17) WTD (all other negative sample results are shown in Supplementary Table S2, Supplementary Figure S1 and S2) and (b) tenfold dilutions of ear tissue homogenates (ID 1,4,11). Samples are grouped by WTD IDs on the x-axis. Data points represent mean AFR ± standard deviation of 8 technical replicates. Negative controls (NC) represent the same sample types. (c–f) Scatterplots with fitted linear regression line with 95% confidence intervals comparing AFR relationships between (c) RPLN to ear samples, (d) tick to ear samples, (e) RPLN to tick samples, or (f) pooled tick samples with pooled tick sample weight in milligrams (mg). Each point represents the mean AFR of 8 technical replicates from WTD ID 1–15. (g–i) Western blot analysis of PMCA products to assess the presence of prion seeding activity for; (g) 14 pooled tick samples (WTD IDs 2–15) stored in RT-QuIC sample buffer evaluated in “a”; (h) 10% tick homogenates (ID 17–19 are NCs); (i) serial dilutions of a CWD-positive (CWD+) brain homogenate (BH) (PMCA positive control), and unseeded (UN) or cellular prion (PrP<sup>C</sup>) (PMCA NCs). (Original uncropped blots/gels are presented in Supplementary Figure S3) Samples analyzed in this figure were tested in duplicate and represent a third PMCA round. Numbers at the right of each panel represent molecular weight markers in kilodaltons (kDa). Red font indicates samples determined to contain PrP<sup>CWD</sup> by either RT-QuIC or PMCA.

of higher AFRs from the corresponding tick samples that we determined to be CWD-positive (Sample IDs 1 (7/8), 4 (7/8), 11 (3/8) (*p*-values 0.0722, 0.0015, 0.0182, respectively, using Dunnett’s Multiple Comparison Test) (Fig. 2a,b). These findings by RT-QuIC indicate a CWD prevalence of 20% (3/15) in *I. scapularis* based on this specific sample of CWD-positive WTD, and suggest that (i) circulation of PrP<sup>CWD</sup> in peripheral tissues is associated with detectable levels of prionemia, which is consistent with previous evaluations of peripheral levels of PrP<sup>CWD</sup> during presymptomatic and symptomatic stages of the disease<sup>22,23</sup> and (ii) that ear tissue or attached and partially or fully engorged ticks may be a less sensitive sample source for CWD diagnostics compared to RPLN using RT-QuIC. Nevertheless, our data indicate that ticks may be considered as an *antemortem* detection method.

While it is possible that the variation observed in seeding activity from peripheral samples compared to RPLN may have been the result of differences in assay sensitivity for the different sample types, it may also be

explained by other factors. The variation observed could have been influenced by the differences in total mass of tick per pooled tick sample; however, no correlation was found between higher or lower AFR values and higher or lower pooled tick samples mass ( $R^2 = 0.02$ ,  $t = 0.46$ ,  $p$ -value = 0.66,  $N = 15$ ; Fig. 2f). Additionally, differences in polymorphisms of the prion protein encoding gene (*PRNP*) can directly influence the rate of disease progression and distribution of PrP<sup>CWD</sup> in WTD<sup>24–27</sup>. The WTD sample size in this study was not large enough to make inferences on how genotype may explain the variable distribution of seeding activity from tick or ear tissue in relation to activity from RPLN. However, genotyping results did show that all ticks from CWD-positive 96G/96S or 96S/96S animals were negative by RT-QuIC (Supplementary Table S1). This is in agreement with the previously suggested delayed accumulation of prions in peripheral tissues by animals harboring 96S alleles<sup>26,27</sup>.

Because the pooled tick samples collected from free-ranging CWD-positive WTD appeared to contain relatively low levels of PrP<sup>CWD</sup> detectable by RT-QuIC, we employed an additional protein amplification assay, the protein misfolding cyclic amplification (PMCA) technique, to further assess the presence of PrP<sup>CWD</sup> in these samples. This assay is akin to RT-QuIC, but uses brain extract from healthy rodents as a source of PrP substrate and relies on cycles of sonication rather than shaking<sup>28</sup> for sensitive and specific detection of PrP<sup>CWD</sup> (Fig. 2i). Relevant to this study, previous reports have shown that PMCA is able to amplify low levels of PrP<sup>CWD</sup> from a wide variety of animal-derived and environmental samples<sup>2,4–6,23,29–33</sup>. From the 30 pooled tick samples collected from CWD-positive and negative WTD previously analyzed by RT-QuIC, PMCA-seeding activity was identified in four samples (Fig. 2g,h). Sample IDs 7, 10, and 15, which were negative based on RT-QuIC seeding activity, showed positive PMCA detection in 1/2 technical replicates. The fourth sample to test positive by PMCA, sample 11 (positive PMCA detection in 2/2 replicates) (Fig. 2g,h), was the only pooled tick sample that was positive based on both assays (Fig. 2a,g,h). Interestingly, this sample also demonstrated the highest seeding activity across all 15 WTD RPLN tested by RT-QuIC and had some of the most sensitive ear tissue seeding activity (Fig. 2a,b). These PMCA results demonstrate a CWD prevalence of 26.7% in *I. scapularis* based on this specific sample of CWD-positive WTD. However, if we consider where the detection of PrP<sup>CWD</sup> agreed between the two amplification assays, the prevalence was only 6.7%.

Because titers of PrP<sup>CWD</sup> from a CWD-positive brain are similar to those found in CWD-positive RPLN<sup>34</sup>, we were able to first extrapolate predicted values for the mass of seeding material present in each RT-QuIC, CWD-positive pooled tick sample (Fig. 3). Then, based on the predicted mass of seeding material present and the previously reported minimum oral ID<sub>50</sub> of CWD-positive brain<sup>35</sup>, we further estimated an ID<sub>50</sub> for ticks from WTD samples 1, 4, and 11 to be 0.3, 42.4, and 6.9, respectively (Eqs. (1) and (3) in Data Analysis, Supplementary Table S3). These estimations suggest that a single *I. scapularis* tick taking a blood meal (i.e., fully, or partially engorged) from a CWD-positive WTD poses a risk to naïve individuals if consumed during social interactions.

## Discussion

Natural modes of indirect transmission of CWD among free-ranging cervids remain poorly examined and may perpetuate endemic increases and broad geographic spread of the disease<sup>1</sup>. The presence of PrP<sup>CWD</sup> in blood may pose a risk for indirect transmission by way of hematophagous ectoparasites acting as mechanical vectors, as cervids can carry high tick infestations and exhibit allogrooming, a common tick defense strategy between conspecifics. However, the role of ticks as mechanical vectors of CWD remains unclear. Here, we demonstrate that a single adult *I. scapularis* found feeding on a CWD-infected WTD may contain approximately 0.3–42.4 ID<sub>50</sub>. These findings suggest that consumption of ticks by deer during bouts of allogrooming may facilitate oral exposure of PrP<sup>CWD</sup> from ticks that consumed blood meals from CWD-infected deer. We demonstrate with artificial membrane feeding assays that *I. scapularis* has the capacity to ingest and excrete PrP<sup>CWD</sup> and sensitivity and specificity of PrP<sup>CWD</sup>-exposed ticks with RT-QuIC validates the presence or absence of PrP<sup>CWD</sup> in wild-fed ticks. Our results show that RT-QuIC seeding activities in wild-fed ticks were analogous to 10–1000 ng of CWD-infected RPLN from each animal (Fig. 3) and peripheral samples were less sensitive using RT-QuIC compared to RPLN (Fig. 2a). Using both RT-QuIC and PMCA, we showed seeding activity in 6 (4 by PMCA, 3 by RT-QuIC, 1 by both) of 15 pooled tick samples removed from wild CWD-infected white-tailed deer (Fig. 2a,g,h). These

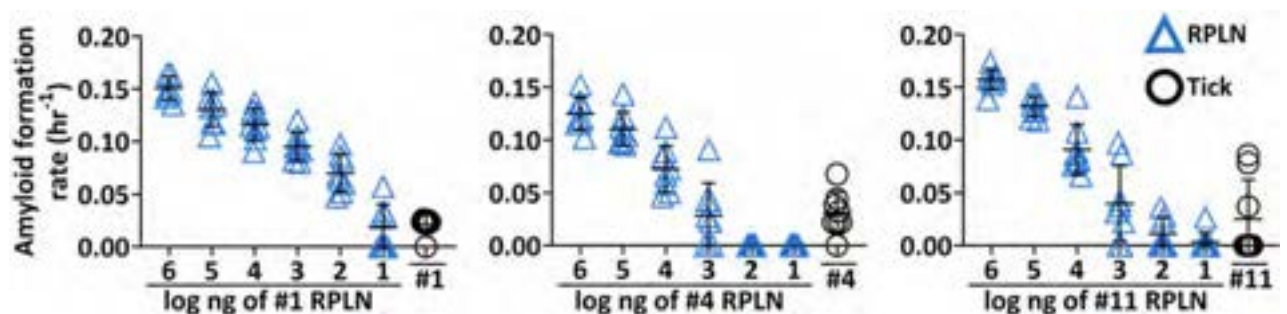


**Figure 3.** Comparison of chronic wasting disease (CWD) prion (PrP<sup>CWD</sup>) loads by *Ixodes scapularis* following infected blood meal with retropharyngeal lymph node (RPLN) from free-ranging white-tailed deer (WTD). Comparisons of relative PrP<sup>CWD</sup> loads present in three separate pooled tick homogenates (ID numbers 1, 4, 11) from Fig. 2a, which tested CWD-positive by our parameters, against a tenfold dilution series of RPLN from corresponding WTD. Data points for 8 technical replicates are depicted for each sample  $\pm$  standard deviation.

results indicate CWD prevalence ranging from 7 to 40% in *I. scapularis* that had fed on CWD-infected WTD and suggest that (i) the amount of PrP<sup>CWD</sup> present in tick samples were near the detection threshold for each method and (ii) that when the amount of PrP<sup>CWD</sup> present in a given sample is relatively low, multiple methods increase the chance of detection in ticks.

Although the ultra-sensitive capabilities of both RT-QuIC and PMCA are well established for detection of misfolded prions in blood from experimental and naturally occurring prion disease<sup>8,21,36</sup> and lymph and skin tissues<sup>37,38</sup>, we observed variation between the two amplification assays in which pooled tick samples were determined CWD-positive (Fig. 2a,g,h). While both RT-QuIC and PMCA are clearly capable of detecting misfolded prions from blood samples, an understanding of how blood-engorged tick extracts behave in either assay is limited. Some sample types have highly sensitive and specific detection (e.g., RPLN), while others have lower sensitivity—often attributed to reaction inhibitors, depending on sample type and amplification assay, necessitating sample or assay optimization to improve sensitivity (e.g., saliva)<sup>39</sup>. Our optimization methods for both whole blood and blood-engorged ticks allowed for sensitive and specific detection of PrP<sup>CWD</sup> from both sample types by RT-QuIC for the spiking experiments (Fig. 1a,h). However, whole blood contained within the engorged ticks may have influenced assay sensitivity, as whole blood components have been shown to inhibit detection of misfolded prion by RT-QuIC<sup>40</sup> and PMCA<sup>41</sup>, which may explain the sensitivity differences between the two assays. The PMCA assay has been utilized to readily detect misfolded prions in blood seemingly without the need for extensive optimization to overcome inhibitors<sup>23</sup> and was therefore used in this study to cross analyze the pooled engorged tick samples tested by RT-QuIC. Although we were able to detect the presence of PrP<sup>CWD</sup> in pooled engorged tick samples by PMCA as well as RT-QuIC, the samples only detected a single sample in common. This relative inconsistency in sample detection between assays could be due to low circulating levels of misfolded prions, which is known to result in lower and inconsistent assay sensitivity<sup>42</sup>. Therefore, it is possible that the differences in sensitivity between RT-QuIC and PMCA observed in this study for detecting PrP<sup>CWD</sup> from wild-fed tick samples may have been the result of low circulating levels of PrP<sup>CWD</sup> in blood, hence low amounts of PrP<sup>CWD</sup> present in tick samples. Additional research in this area could determine the comparative power of these two techniques for this specific sample type.

We fully recognize that the 10<sup>-3</sup> mg/mL dilution used for the spiking blood meals for the membrane feeding assays is not typical of what is found in blood of early or late-stage CWD-infected deer and that based on results from McNulty et al.<sup>21</sup>, the relative concentration of prions in blood is likely ~ 3 orders of magnitude lower than a 10<sup>-3</sup> mg/mL concentration of CWD-positive brain. However, considering results published by Shikiya et al.<sup>12</sup>, which found no uptake of prions by nymphal Rocky Mountain wood ticks (*Dermacentor andersoni*) following an animal challenge study, we felt it necessary to use such high concentrations of CWD-positive spiking material to demonstrate the capacity of *I. scapularis* to assimilate prions from a blood meal rather than demonstrate natural uptake under the most ideal controlled conditions. Future studies considering both—blood specimens spiked with more diluted prion titers (mimicking prion concentrations at different stages of the animal's disease course) and blood from actual deer—would be important to consider when evaluating assay sensitivity between PMCA and RT-QuIC.

The observation of inconsistencies of seeding activity by ear or tick samples compared to seeding activity of RPLN from the 15 CWD-positive WTD may be the result of differences in the stage of CWD disease progression across the individuals sampled, as variation in disease stage could influence PrP<sup>CWD</sup> distribution<sup>43</sup>. Although we cannot confirm disease stage for any of the sampled WTD included in this study, this sample set of WTD was not randomly selected, but rather based on those selectively harvested by hunters, making it unlikely that any of the sampled individuals were in the end-stages of CWD. Hence, there is an expectation that the ear tissue and pooled tick samples would contain relatively low PrP<sup>CWD</sup> levels, given lower blood flow to ear tissue, the small sample volumes taken up by adult ticks, and that it is unlikely that a deer in the terminal stage of CWD would have been targeted for hunter harvest. Although PMCA and RT-QuIC are capable of detection of misfolded prions at femtogram levels—similar to the lower detection limit of bioassay<sup>44,45</sup>—the inconsistencies in sensitivity between the two assays for our sample set may have resulted from having samples that contain PrP<sup>CWD</sup> levels below detection thresholds for even these ultra-sensitive amplification assays. This possible detection limit may explain why WTD 11 was the only deer with a pooled tick sample that overlapped in positivity between the two assays (Fig. 2a,g,h). The elevated RPLN AFRs and more sensitive seeding of ear tissue from sample 11 compared to all other RPLN and ear tissue samples suggests that this individual had higher circulating amounts of PrP<sup>CWD</sup> levels that were at or above the detection threshold between the two assays (Fig. 2a,b). Future work aimed at better understanding how the range of PrP<sup>CWD</sup> levels that ticks may harbor affects assay sensitivity and detection rates could incorporate a broader sample set that includes samples from deer that are in the end-stages of CWD. Additionally, this study only investigated ticks concentrated around the head and neck of deer. It is possible that ticks collected from other anatomical regions lacking a common vasculature with the head may exhibit different PrP<sup>CWD</sup> detectability and prevalence. Further studies investigating engorged ticks across the entire anatomy of WTD are warranted.

While variation of seeding activity observed in pooled tick and ear tissue samples across the individual free-ranging WTD from this study may demonstrate limits of detection for both PMCA and RT-QuIC, the naturally occurring PrP<sup>CWD</sup> loads from ticks and ear tissue collected from the 15 CWD-positive WTD may also be influenced by *PRNP* genotype<sup>27</sup>. Although the small sample size of CWD-positive animals in this study limited our ability to assess how genotype alters variation in seeding activities, we found that RT-QuIC tested pooled tick samples from CWD-positive 96G/96S or 96S/96S animals were negative and positive pooled tick samples came from CWD-positive 96G/96G. The four positive PCMA results for the same pooled tick samples showed detection of PrP<sup>CWD</sup> from one CWD-positive 96G/96S, and three CWD-positive 96G/96G (See Supplementary Table S1 for genotype results and more information regarding genotypes). An additional consideration is that CWD strain variation may be another plausible explanation for the distribution in seeding activity across the

sample types examined in this study, as peripheral and neural PrP<sup>CWD</sup> distribution can differ across recognized CWD strains<sup>46</sup>.

Indirect transmission routes of CWD likely play an important role in CWD disease dynamics<sup>1</sup> and are quite possibly a combination of various modes of exposure that may include consumption or inhalation of contaminated soil<sup>47,48</sup>, consumption of contaminated plant matter<sup>4</sup>, or mucosal contact with contaminated fomites or other environmental materials<sup>49</sup>. Few studies have utilized RT-QuIC to evaluate the involvement of other species in the ecological community that may influence CWD exposure or transmission. We have identified a potential mechanical vector of CWD not previously evaluated for WTD, with implications for host behavior that may influence CWD exposure events. We recognize that experimentally-determined oral ID<sub>50</sub> of our tick samples may vary significantly from our estimates, as it is quite evident different prion loads were present in each animal based on the RPLN dilution series (Fig. 3), and the prior study<sup>35</sup> used to estimate the ID<sub>50</sub> utilized a pool of infectious material generated from laboratory-infected late-stage animals. As such, these can be considered preliminary estimates for ID<sub>50</sub> in ticks; our sample size is small and experimentation in mouse models would establish a true ID<sub>50</sub>. Nevertheless, our findings suggest that infection relevant loads of seeding material are indeed present in individual ticks, likely within an order of magnitude of 1 ID<sub>50</sub>. These findings and implications may prove useful for CWD research and adaptive management efforts moving forward as we advance our understanding of ecologically relevant drivers of CWD dynamics. Future studies could clarify the prevalence of CWD in ticks for a single deer and explore the potential importance of the relationship between tick CWD prevalence and where on the host's body the tick attaches. Although the detection rate varied depending on the seeded amplification assay being used, this was not surprising as it is well known that biological and environmental specimens may carry components affecting the PrP<sup>C</sup>–PrP<sup>CWD</sup> conversion process. Future studies could determine whether sample pre-treatments or modifications in the RT-QuIC or PMCA processes increase prion detection ratio in ticks and other parasites. Importantly, future research including bioassays, evaluating larger samples sizes of *I. scapularis* and other tick species collected from WTD, and additional wild cervid species across different regions of North America would expand our understanding of the role that blood obligate ectoparasites and associated biogeographical factors may have on CWD dynamics. For example, land use change and shifts in regional climate regimes may result in higher tick infestations on cervids and contemporary range expansion for different tick species<sup>50</sup>, potentially increasing the likelihood of this type of exposure event among WTD and other cervids. Additionally, behavioral studies evaluating cervid allogrooming frequency, rate, and preferences for allogrooming across different cervid species could shed light on links between host behavior, disease status and conspecific exposure risk. For example, do end-stage CWD-infected cervids accumulate higher tick burdens (suggested in<sup>51</sup>) through altered grooming or habitat selection behaviors? Do healthy individuals continue to groom infected conspecifics or do they avoid allogrooming interactions with visibly sick individuals? Future research efforts could help elucidate the impact of ticks and grooming behaviors on transmission of CWD in free-ranging cervids.

## Methods

**Membrane fabrication and feeding chamber assembly.** The tick artificial membrane-feeding method used was based on Oliver et al.<sup>20</sup>, with some modifications. Briefly, silicone membranes were produced by infiltrating 50% rayon and 50% cellulose microscope lens paper (Matin) with a two-component liquid silicone rubber with a shore hardness of 00–50 (Ecoflex Supersoft 0050, Smooth-On, PA, USA), mixed 1:1 and thinned by adding 1.5 mL hexane into 10 mL silicone mixture (Fig. 1e). The lens cleaning paper was taped to a flat, plastic wrap-lined surface and the silicone mixture scraped over the lens cleaning paper to obtain a membrane with a thickness of ~70–100 µm. Membrane thickness was determined by measuring 4–6 points on each cured membrane with a micrometer. Membranes were allowed to cure overnight before feeding chamber attachment using a 1:1 mixture of a two-part silicone glue with shore A hardness of 30 (Mold Star 30, Smooth-On) as previously described, resulting in 4–6 feeding chambers per cured membrane sheet (Fig. 1i). Assembled feeding chambers were cured overnight, trimmed with a scalpel, and leak-tested by adding 5 mL of sterile water to each chamber for at least 1 h, discarding any leaky membranes. To ensure feeding chambers remained upright and membranes were submerged into blood-containing wells, plastic graduated cylinder bumpers were placed around feeding units and glued into place with silicone glue (Gorilla Glue) (Fig. 1f,g).

**Tick housing and feeding.** Pathogen free *I. scapularis* male and female adults were acquired from the Oklahoma State Tick Rearing facility, Stillwater, Oklahoma, U.S.A., and housed in a humidity chamber (Durable, 64-quart clear storage tote with lid) at 24 °C with 97–99% relative humidity (Durac, hygrometer). Humidity was maintained by placing lidless, smaller separate plastic containers containing a saturated potassium sulfate solution (~0.5 kg K<sub>2</sub>SO<sub>4</sub> (potassium sulfate) submerged in ~500 mL of sterile deionized water) within the larger humidity chamber. Ticks were acclimated to the humidity chamber for ~5 h prior to starting artificial membrane feeding. Sterile, mechanically defibrinated bovine blood (Hemostat Laboratories, Dixon, CA) was used. Three mL of blood supplemented with 4.5 µL of 3 mM ATP was prewarmed to 37 °C, then added to each well of a six-well plate to stimulate feeding<sup>52</sup>. In total 10–14 female and 5–7 male *I. scapularis* were placed in each feeding chamber enclosed using a fine synthetic mesh fabric (Anteer Crystal Organza, China), fixed in place with a tight rubber band. If available from previous feedings, 10–15 granules of tick frass were added to each feeding chamber as a feeding stimulant. Feeding chambers were positioned in direct contact with the blood without trapping air bubbles between the membrane and the blood, submerging membranes by at least 2 cm. Each plate was placed afloat in a 37 °C water bath in a room that provided a 16:8 h photoperiod. Every 24 h, blood was replaced by placing 3 mL of prewarmed bovine blood as described above in a new six-well plate. To remove the build-up of blood residue from the previous day's feeding, the outer surface of each feeding chamber and

membrane that were in contact with the blood were vigorously rinsed with sterile 1X phosphate-buffered saline (PBS) using a pipette.

**Exposure of *I. scapularis* to CWD by membrane feeding.** To determine tick uptake of PrP<sup>CWD</sup> from inoculated blood meals, we inoculated 2.970 mL of defibrinated bovine blood with a 30  $\mu$ L of a 10% (w/v) CWD-positive WTD brain homogenate (from the obex region; sourced from Wisconsin Department of Natural Resources (WDNR) tagged WTD #5219) prepared in 1X PBS to achieve a final concentration of  $10^{-3}$  mg/mL of CWD-positive brain for the CWD-positive treatment group. For the negative control treatment group, 2.970 mL defibrinated blood was treated with 30  $\mu$ L of 1X PBS. Separate six-well plates were used for each treatment group and each six-well plate with feeding chambers attached were placed afloat in a 37 °C water bath that was housed within a humidity chamber (24 °C with 97–99% relative humidity). Every 24 h, feeding unit plates were replaced and refilled with fresh blood for each treatment group. The outer surfaces of the feeding chamber and membranes were washed as detailed above, washing the negative control feeding units first and the CWD-positive treatment feeding chambers last to prevent any possibility for cross contamination. Ticks were allowed to feed to repletion for ~9–14 days, during which frass was also collected from each treatment group. Engorged, detached ticks and frass were stored at –20 °C prior to preparation for RT-QuIC or PMCA analyses.

**Collection of ear tissue and ticks attached to hunter harvested, wild white-tailed deer.** Through cooperation with the WIDNR CWD processing center, heads of voluntarily submitted hunter-harvested WTD from several Wisconsin counties were manually examined for ticks from October 2021 to December 2021. Examinations generally consisted of combing fingers through pelage for attached ticks on each WTD head while wearing nitrile gloves. When detected, attached ticks were removed, typically found on the outer ear, brow, chin, cheek, snout, or neck regions. Each head was contained within a leak-proof disposable plastic bag and tagged with a WIDNR barcode for identification and linking to metadata for CWD testing. To prevent cross contamination of each deer head being examined, heads were kept within their respective bags, gloves were changed between each head examination, and a new sterile scalpel was used for removal of the entire left ear of each head. Each ear sample was placed in a sterile Whirl-Pak bag (Nasco, 48,137), and any ticks collected from a given head were collectively placed in sterile 1.5 mL snap-cap centrifuge tubes. All samples were labeled with the respective barcodes for each head examined, and the number and species of tick collected from CWD-positive WTD were cataloged. Tissue and tick samples were stored at –20 °C prior to preparation for use in the RT-QuIC or PMCA assays.

**Tick, blood, and frass homogenate preparations for RT-QuIC.** To prepare tick homogenates, a mix of partially and fully engorged *I. scapularis* female ticks equaling a total weight of ~200 mg (unless stated otherwise, equivalent to ~142  $\mu$ L of blood meal), were placed in a ring-sealed 1.5 mL centrifuge tube with ~30–40 0.7 mm zirconia beads (BioSpec) with 1 mL of PBS and processed at room temperature in a bead mill homogenizer (Fisherbrand Bead Mill 24) on the highest setting (setting six) for 3 min. The mass of each tick sample collected from hunter-submitted deer heads varied and was therefore prepared using volumes of 1X PBS to result in a 10% (w/v) homogenate. Next, tick homogenates were mixed with chitinase (1 mg/mL final concentration) (Sigma-Aldrich Cat. # C824) and allowed to digest in a thermomixer (1,400 rpm, 24 h, 45 °C; Eppendorf ThermoMixer F1.5). Following digestion, Lipase AY30 (100  $\mu$ g/mL final concentration; Acros Organics) was added, and homogenates were thermomixed for 1 h (37 °C, 1400 rpm; Eppendorf ThermoMixer F1.5), followed by centrifugation (25 °C, 15 min, 16,000 $\times$ g). Supernatants were collected, centrifuged again to ensure sample clarification (25 °C, 15 min, 16,000 $\times$ g), mixed 1:1 with 23.1 mM sodium phosphotungstate hydrate (Na-PTA) (Sigma-Aldrich, Cat. # 496,626), incubated without agitation for 16 h at 4 °C. Samples were then centrifuged (4 °C, 30 min, 5000 $\times$ g), pellets were retained and washed with a 1:1 solution of 18 M $\Omega$  H<sub>2</sub>O and 23.1 mM sodium phosphotungstate (Na-PTA) followed by centrifugation (4 °C, 30 min, 5000 $\times$ g) and aspiration of the wash solution. Pellets were resuspended in 30  $\mu$ L of RT-QuIC sample buffer (0.1% SDS in 1X PBS and N2 supplement (Gibco, 17,502,048)) using sonication (1 min, amplitude 36; Qsonica Q-700), and 2  $\mu$ L was used to seed each reaction well of the 96 well-plate for the RT-QuIC assay. Eight technical replicates were used per biological replicate, unless stated otherwise.

For spiking experiments using tick homogenates for RT-QuIC optimization, the initial volume of the spiked sample consisted of 450  $\mu$ L of negative control tick homogenate (as prepared above), 450  $\mu$ L chitinase (1 mg/mL final concentration), and 100  $\mu$ L of a  $10^{-3}$  dilution of either CWD-positive or CWD-negative WTD brain. Then the steps outlined above for preparing tick homogenates were performed, with Na-PTA pellets resuspended in 100  $\mu$ L and ten-fold dilutions were prepared from the  $10^{-3}$  spiked sample. Two  $\mu$ L of each dilution were used to seed each reaction well for eight technical replicates. Spiking experiments used to demonstrate recovery of PrP<sup>CWD</sup> from defibrinated bovine blood were carried out using 200  $\mu$ L of blood combined with 1 mL PBS, followed by the homogenization step with an additional 1 mL of PBS added. The initial volume of the spiked blood samples consisted of 450  $\mu$ L blood homogenate, 450  $\mu$ L PBS, and 100  $\mu$ L  $10^{-3}$  CWD-positive of CWD-negative WTD brain homogenate dilution. Samples were incubated in a thermomixer for 16 h (45 °C, 1400 rpm), then 1.5  $\mu$ L of Lipase AY30 (100  $\mu$ g/mL final concentration; Acros Organics) was added and the samples homogenized with Na-PTA pellets resuspended in 100  $\mu$ L of RT-QuIC sample buffer and tenfold dilutions were prepared from the  $10^{-3}$  spiked sample, using 2  $\mu$ L of each dilution to seed each reaction well for eight technical replicates per biological replicate. For RT-QuIC analysis of tick frass from feeding experiments, 70 mg of frass from each treatment group was added to 1 mL of 1X PBS, followed by homogenization. Lipase AY30 (100  $\mu$ g/mL final concentration) was added, and samples were incubated in a thermomixer for 1 h (37 °C, 1400 rpm), centrifuged (16,000 $\times$ g, 15 min, 25 °C), and supernatants were collected. Next, 500  $\mu$ L of 1X PBS was added to 500  $\mu$ L of the

supernatant, then mixed 1:1 with 23.1 mM sodium phosphotungstate followed by incubated without agitation for 16 h at 4 °C. Na-PTA pellets were centrifuged, washed, and centrifuged again, then resuspended in 30  $\mu$ L with sonication. Then, 2  $\mu$ L of each sample was used to seed each reaction well for 8 technical replicates.

**Tissue homogenate preparation for RT-QuIC.** Ear tissue was prepared as described in Burgener et al.<sup>53</sup>. Briefly, 100 mg of ear tissue collected from the central area of the pinna was placed in a digestion solution (1X PBS, 2 mM CaCl<sub>2</sub> (Dot Scientific DSC20010-1000), and collagenase A (2.5 mg/mL final concentration) (Sigma-Aldrich 10,103,586,001)) were homogenized with a bead beater (1 min, 4 m/s; Fisherbrand Bead Mill 24) and 0.7 mm diameter zirconia beads (BioSpec). These samples were then further processed with a thermomixer (1400 rpm, 24 h, 45 °C; Eppendorf ThermoMixer F1.5), after which they were centrifuged (2 min, 3000 $\times$ g), and the supernatants retained. The supernatants were centrifuged again (3 min, 3000 $\times$ g) to remove any small particulate matter, aliquoted, and frozen at – 20 °C until use for RT-QuIC analysis.

**Real-time quaking-induced conversion assay.** The RT-QuIC in vitro protein amplification assay was performed as described by Metrick et al.<sup>54</sup> with minor modifications. Briefly, 2  $\mu$ L of sample extracts were added to a given well of a 96-well format optical-bottom black microplate (Fisher), each already containing 98  $\mu$ L of RT-QuIC reaction mixture (0.1 mg·mL<sup>-1</sup> 90–231 recombinant hamster prion protein (produced as previously described by Orru et al.<sup>55</sup>, 300 mM sodium iodide, 20 mM sodium phosphate, 1.0 mM ethylenediaminetetraacetic acid, and 10  $\mu$ M thioflavin T). Microplate-compatible spectrophotometers capable of heating, shaking, and fluorescence monitoring (BMG FLUOstar, Cary, NC) were used with the following instrument settings: 50 °C for spiked samples (unless described otherwise) double orbital pattern shaking at 700 rpm with 60-s shake/60-s rest cycles, fluorescent scans ( $\lambda_{\text{excitation}} = 448$  nm,  $\lambda_{\text{emission}} = 482$  nm) every 15 min, at a gain of 1600, and a total run time of 48 h.

**CWD status by ELISA.** Retropharyngeal lymph nodes collected from hunter-harvested deer were tested by enzyme-linked immunosorbent assay (ELISA) using the standard protocol approved by the U.S. Department of Agriculture (USDA) at the Wisconsin Veterinary Diagnostic Center, Madison, Wisconsin, U.S.A. The ELISA assay was conducted using a commercial Transmissible Spongiform Encephalopathy Antigen Test kit (Bio-Rad, Catalogue# 12,004,413) (bovine obex or mule deer/WTD/elk RPLN and obex), following manufacturer's instruction. Identification of the presence of CWD is based on an optical density (OD) value that is equal to or greater than the USDA cut-off value (0.035).

**Protein misfolding cyclic amplification.** The PMCA substrate was generated from a pool of brains from Tg(CerPrP)<sup>1536<sup>+/+</sup>56</sup> mice as described in Morales et al.<sup>28</sup>. PMCA substrate was supplemented with digitonin (Invitrogen, Carlsbad, CA, USA) and EDTA (Promega, Madison, WI, USA) at final concentrations of 0.025% and 6 mM, respectively. Aliquots of 90  $\mu$ L of PMCA substrate were transferred in 0.2 mL PCR tubes strips (Eppendorf, Enfield, CT, USA) containing PTFE beads (Engineering Laboratories, Inc., Oakland, NJ, USA) and mixed with 10  $\mu$ L of tick-derived samples. Tick samples used for PMCA were prepared in either RT-QuIC sample buffer or as a clarified homogenate following treatment with chitinase, Lypase AY30, and centrifugation to further clarify the sample prior to adding Na-PTA as described above in the “[Tick, blood, and frass homogenate preparations for RT-QuIC](#)” section above. The PMCA reactions were submitted to a first round of 144 cycles of incubation/sonication. The resulting PMCA products (10  $\mu$ L) were mixed with fresh PMCA substrate supplemented (90  $\mu$ L) and subjected to two additional PMCA rounds of 96 cycles each. Each PMCA cycle consisted of 29 min., and 40 s of incubation, and 20 s of sonication at 37 °C. Each PMCA reaction set included PMCA reactions spiked with serial dilutions of CWD-positive brain (10  $\mu$ L) of known PMCA activity and 4 unseeded reactions as negative controls. PMCA products were mixed with proteinase K (PK, Sigma-Aldrich, Saint Louis, MO, USA) at final concentration of 100  $\mu$ g/mL and incubated at 37 °C for 90 min with shaking. The PK catalytic activity was stopped by adding NuPAGE LDS sample buffer (Invitrogen, Carlsbad, CA, USA) at final concentration of 1X and heated at 90 °C for 10 min. PK-treated PMCA products were visualized by western blot using the Bar-224 antibody (Bertin Corp, Rockville, MD, USA) at 1:10,000 dilution. PMCA manipulators were blinded to the identity of the samples.

**PRNP analysis.** Genomic DNA was extracted from ~ 100 mg of ear tissue from 17 out of 30 WTD included in this study using methods outlined in Green and Sambrook, 2012 for phenol–chloroform extraction and ethanol precipitation<sup>57</sup>. An approximately 750 bp PRNP gene sequence was amplified by conventional PCR and sequenced at the University of Wisconsin Biotechnology Center (Madison, Wisconsin, U.S.A) using primer sequences developed by O'Rourke et al.<sup>24</sup>. PCR sequences were then aligned and evaluated using Unipro UGENE software version 42.0 ([www.ugene.net](http://www.ugene.net)). Specific single nucleotide polymorphisms at position 95 (glutamine [Q] or histidine [H]), 96 (glycine [G] or serine [S]) were identified and recorded. Although an updated set of primers which accounts for rare PRNP alleles was recently identified<sup>58,59</sup> following the initial submission of our findings, primers used for this study have demonstrated consistent utility for the past decade<sup>25,60</sup>.

**Data analysis.** Data were analyzed and visualized using Jmp Pro 15 (SAS Institute, Cary, NC) and Prism 8 (GraphPad, San Diego, CA). Thresholds used to determine AFRs were calculated by adding twenty times the standard deviation of the relative fluorescence unit (RFU) values from cycles 3–14 to the mean of RFU values from cycles 3–14 to account for baseline variation amongst samples and to apply a rigorous standard for distinguishing true positive samples from true negatives.

We first evaluated if we could recover and detect PrP<sup>CWD</sup> from spiked tick homogenates or spiked blood as compared to the source material (CWD-positive brain tissue), and if the recovery rates differed by sample type. We used a two-way (factorial) analysis of variance (ANOVA) to compare AFR values among sample types (CWD-positive brain, spiked-blood or spiked tick homogenates). We included an interaction between sample type and sample dilution, to assess if detection/recovery in different sample types was sensitive to the sample concentration across the tenfold dilution series.

After this proof of concept, we then evaluated whether ticks experimentally fed blood inoculated with CWD-positive BH could ingest and excrete prions. We used a two-way (factorial) ANOVA to assess differences in AFR values based on sample type (CWD-positive brain tissue, ticks fed prion-spiked blood, or frass from the experimentally-fed ticks) and the interaction between sample type and sample dilution across the tenfold dilution series.

To analyze whether PrP<sup>CWD</sup> was detectable in engorged ticks collected from free-ranging CWD-positive deer, we compared results generated by two protein amplification assays, RT-QuIC and PMCA. Pooled tick samples amplified by PMCA that demonstrated bands between 34 and 26 kDa were interpreted as being positive for having PrP<sup>CWD</sup> present<sup>61</sup>. Pooled tick samples analyzed by RT-QuIC were considered positive if a sample had at least 3 out of 8 technical replicates with seeding activity and also by statistical analysis, using Dunnett's multiple comparison test of AFR values to distinguish which pooled tick samples were significantly different from the negative control pooled tick samples collected from free-ranging CWD-negative WTD heads.

Since CWD testing in free-ranging cervids currently relies upon invasive sampling of RPLN, we explored if CWD status could be assessed through more readily accessible tissues (such as ear tissue or ectoparasites) which could provide support for performing less invasive *antemortem* CWD testing. Therefore, we collected RT-QuIC average AFR values for three sample types (lymph node, ear, or pooled tick samples) from individual deer to evaluate if AFR values were correlated (i.e., do deer with high AFR values in lymph nodes have higher AFR values in ear or tick samples than deer with lower AFR values?). Using linear regressions, we explored relationships between average AFRs for the three sample types collected from the CWD-positive deer in our sample set.

We then calculated if prion concentrations detected in ticks from free-ranging deer had the potential to be infectious, based on estimates of the amount of prion seeding material in our samples relative to an experimentally-determined ID<sub>50</sub> for an equivalent amount of prion seeding material in brain<sup>35</sup>. To estimate a predicted per-tick ID<sub>50</sub> (ID<sub>50P</sub>) we need to know the ng of predicted seeding material per 1 mg of tick for a pooled sample (*S*), the average mass (mg) for a single tick from a pooled sample (*m*) from WTD ID 1, 4, and 11, and the actual ID<sub>50</sub> of an equivalent mass of CWD-positive brain (300 ng = ID<sub>50A</sub>):

$$ID_{50P} = (S \times m) \div ID_{50A} \quad (1)$$

Titers of PrP<sup>CWD</sup> from a CWD-positive brain are similar to those found in CWD-positive RPLN<sup>34</sup>, and a recent study has described a minimum mass of 300 ng of CWD-positive brain derived from a pool of 6 CWD-positive deer to be an effective oral ID<sub>50</sub> for WTD<sup>35</sup>. As such, to calculate *S*, we first modeled, using a sum of exponential functions, the AFR values generated for the tenfold dilution series using mass of RPLN tissue per 2 μL (the amount of sample used to seed each well) for each of the RPLN samples (1, 4, and 11) as the explanatory variable. Thus, our global model was:

$$AFR_i = a + b \times \exp(-d \times ng_i) + c \times \exp(-f \times ng_i), \quad (2)$$

where  $AFR_i$  is the observed AFR for the  $i$ th observation,  $a$ ,  $b$ ,  $c$ ,  $d$  and  $f$  are parameters that are estimated and  $ng_i$  is the mass of sample for the  $i$ th observation. Parameters for each model were estimated using a least squares loss function within the Nonlinear Fit Curve Personality of Jmp Pro 15 (SAS Institute, Cary, NC). For each dataset we examined a suite of 4 models, which were based on the global model described above with either 2, 3, 4, or 5 parameters. We used the Akaike information criterion (AIC<sub>c</sub>) corrected for small sample size, to select which model from this suite of models provided the most parsimonious fit for each of the three RPLN data sets. (see Supplementary Table S4 and S5 for AIC<sub>c</sub> values and associated suite of models examined)<sup>62</sup>. Based on AIC<sub>c</sub> values, the global 5-parameter model was chosen for data for sample #1 and the 4-parameter model best fit data for samples #4 and 11. The fitted models were then used as calibration curves to predict the relative amount of seeding material present in 2 μL of each pooled tick sample (For full model equations see Supplementary Table S4). Therefore, if  $ng_p$  is the predicted mass of seeding material in a 30 μL volume (the total volume of prepared pooled tick sample in RT-QuIC sample buffer, see Supplemental Material Methods section), and  $M_t$  is the total mass of (mg) of a pooled tick sample, then *S*, the ng of seeding material per 1 mg of tick for a pooled sample, is estimated as:

$$S = (ng_p) \div (M_t) \quad (3)$$

**Ethics approval.** All animal manipulations were approved by the Animal Welfare Committee (AWC) at The University of Texas Health Science Center at Houston. Protocol number AWC-20-0065. All procedures were conducted following Federal and University guidelines. All methods are in accordance with ARRIVE guidelines. Mice were bred in approved facilities and euthanized by CO<sub>2</sub> inhalation. The experiments listed in this manuscript did not involve animal experimentations and only tissues from euthanized mice were used as reagents for the PMCA reactions.

### Data availability

The datasets generated and/or analyzed during the current study<sup>63</sup> are available at [www.sciencebase.gov](http://www.sciencebase.gov) using <https://doi.org/10.5066/P9CAMSWN>.

Received: 12 October 2022; Accepted: 27 April 2023

Published online: 15 May 2023

## References

- Almberg, E. S., Cross, P. C., Johnson, C. J., Heisey, D. M. & Richards, B. J. Modeling routes of chronic wasting disease transmission: Environmental prion persistence promotes deer population decline and extinction. *PLoS ONE* **6**, e19896. <https://doi.org/10.1371/journal.pone.0019896> (2011).
- Kramm, C. *et al.* In vitro detection of chronic wasting disease (CWD) prions in semen and reproductive tissues of white tailed deer bucks (*Odocoileus virginianus*). *PLoS ONE* **14**, e0226560. <https://doi.org/10.1371/journal.pone.0226560> (2019).
- Johnson, C. J. *et al.* Prions adhere to soil minerals and remain infectious. *PLoS Pathog.* **2**, e32. <https://doi.org/10.1371/journal.ppat.0020032> (2006).
- Pritzkow, S. *et al.* Grass plants bind, retain, uptake, and transport infectious prions. *Cell. Rep.* **11**, 1168–1175. <https://doi.org/10.1016/j.celrep.2015.04.036> (2015).
- Nichols, T. A. *et al.* Detection of protease-resistant cervid prion protein in water from a CWD-endemic area. *Prion* **3**, 171–183. <https://doi.org/10.4161/pri.3.3.9819> (2009).
- Pritzkow, S. *et al.* Efficient prion disease transmission through common environmental materials. *J. Biol. Chem.* **293**, 3363–3373. <https://doi.org/10.1074/jbc.M117.810747> (2018).
- Mysterud, A. *et al.* Antler cannibalism in reindeer. *Sci. Rep.* **10**, 22168. <https://doi.org/10.1038/s41598-020-79050-2> (2020).
- Chen, B., Morales, R., Barria, M. A. & Soto, C. Estimating prion concentration in fluids and tissues by quantitative PMCA. *Nat Methods* **7**, 519–520. <https://doi.org/10.1038/nmeth.1465> (2010).
- Henderson, D. M. *et al.* Detection of chronic wasting disease prion seeding activity in deer and elk feces by real-time quaking-induced conversion. *J. Gen. Virol.* **98**, 1953–1962. <https://doi.org/10.1099/jgv.0.000844> (2017).
- Mathiason, C. K. *et al.* B cells and platelets harbor prion infectivity in the blood of deer infected with chronic wasting disease. *J. Virol.* **84**, 5097–5107. <https://doi.org/10.1128/jvi.02169-09> (2010).
- Wisniewski, H. M., Sigurdarson, S., Rubenstein, R., Kasczak, R. J. & Carp, R. I. Mites as vectors for scrapie. *Lancet* **347**, 1114. [https://doi.org/10.1016/s0140-6736\(96\)90310-4](https://doi.org/10.1016/s0140-6736(96)90310-4) (1996).
- Shikiya, R. A., Kincaid, A. E., Bartz, J. C. & Bourret, T. J. Failure to detect prion infectivity in ticks following prion-infected blood meal. *MSphere* <https://doi.org/10.1128/mSphere.00741-20> (2020).
- Haley, N. J., Henderson, D. M., Senior, K., Miller, M. & Donner, R. Evaluation of winter ticks (*Dermacentor albipictus*) collected from North American Elk (*Cervus canadensis*) in an area of chronic wasting disease endemicity for evidence of PrP(CWD) amplification using real-time quaking-induced conversion assay. *MSphere* **005**, 1521. <https://doi.org/10.1128/mSphere.00515-21> (2021).
- Sonenshine, D., Lane, R. & Nicholson, W. Ticks (Ixodida). In *Medical and veterinary entomology* (eds Mullen, G. R. & Durden, L. A.) 517–558 (Elsevier, 2002).
- Kaufman, W. R. & Phillips, J. E. Ion and water-balance in ixodid tick *dermacentor-andersoni*. 1. Routes of ion and water excretion. *J. Exp. Biol.* **58**, 523–536 (1973).
- Fielden, L. J., Jones, R. M., Goldberg, M. & Rechav, Y. Feeding and respiratory gas exchange in the American dog tick, *Dermacentor variabilis*. *J. Insect Physiol.* **45**, 297–304. [https://doi.org/10.1016/s0022-1910\(98\)00127-9](https://doi.org/10.1016/s0022-1910(98)00127-9) (1999).
- Bueler, H. *et al.* Mice devoid of PrP are resistant to scrapie. *Cell* **73**, 1339–1347. [https://doi.org/10.1016/0092-8674\(93\)90360-3](https://doi.org/10.1016/0092-8674(93)90360-3) (1993).
- Mooring, M. S. & Samuel, W. M. Tick-removal grooming by elk (*Cervus elaphus*): Testing the principles of the programmed-grooming hypothesis. *Can. J. Zool.-Rev.* **76**, 740–750. <https://doi.org/10.1139/cjz-76-4-740> (1998).
- Hirth, D. Social behavior of white-tailed deer in relation to habitat. *Wildl. Monogr.* **53**, 1–55 (1977).
- Oliver, J. D. *et al.* Infection of immature Ixodes scapularis (Acari: Ixodidae) by membrane feeding. *J. Med. Entomol.* **53**, 409–415. <https://doi.org/10.1093/jme/tjv241> (2016).
- McNulty, E. E. *et al.* In vitro detection of haematogenous prions in white-tailed deer orally dosed with low concentrations of chronic wasting disease. *J. Gen. Virol.* **101**, 347–361. <https://doi.org/10.1099/jgv.0.001367> (2020).
- Ferreira, N. C. *et al.* Detection of chronic wasting disease in mule and white-tailed deer by RT-QuIC analysis of outer ear. *Sci. Rep.* **11**, 7702. <https://doi.org/10.1038/s41598-021-87295-8> (2021).
- Kramm, C. *et al.* Detection of prions in blood of cervids at the asymptomatic stage of chronic wasting disease. *Sci. Rep.* **7**, 17241. <https://doi.org/10.1038/s41598-017-17090-x> (2017).
- O'Rourke, K. I. *et al.* Polymorphisms in the prion precursor functional gene but not the pseudogene are associated with susceptibility to chronic wasting disease in white-tailed deer. *J. Gen. Virol.* **85**, 1339–1346. <https://doi.org/10.1099/vir.0.79785-0> (2004).
- Haley, N. J. *et al.* Estimating relative CWD susceptibility and disease progression in farmed white-tailed deer with rare PRNP alleles. *PLoS ONE* **14**, e0224342. <https://doi.org/10.1371/journal.pone.0224342> (2019).
- Johnson, C. J. *et al.* Prion protein polymorphisms affect chronic wasting disease progression. *PLoS ONE* **6**, e17450. <https://doi.org/10.1371/journal.pone.0017450> (2011).
- Otero, A. *et al.* Prion protein polymorphisms associated with reduced CWD susceptibility limit peripheral PrPCWD deposition in orally infected white-tailed deer. *BMC Vet. Res.* <https://doi.org/10.1186/s12917-019-1794-z> (2019).
- Morales, R., Duran-Aniotz, C., Diaz-Espinoza, R., Camacho, M. V. & Soto, C. Protein misfolding cyclic amplification of infectious prions. *Nat. Protoc.* **7**, 1397–1409. <https://doi.org/10.1038/nprot.2012.067> (2012).
- Plummer, I. H., Wright, S. D., Johnson, C. J., Pedersen, J. A. & Samuel, M. D. Temporal patterns of chronic wasting disease prion excretion in three cervid species. *J. Gen. Virol.* **98**, 1932–1942. <https://doi.org/10.1099/jgv.0.000845> (2017).
- Haley, N. J., Mathiason, C. K., Zabel, M. D., Telling, G. C. & Hoover, E. A. Detection of sub-clinical CWD infection in conventional test-negative deer long after oral exposure to urine and feces from CWD+ deer. *PLoS ONE* **4**, e7990. <https://doi.org/10.1371/journal.pone.0007990> (2009).
- Bravo-Risi, F. *et al.* Detection of CWD prions in naturally infected white-tailed deer fetuses and gestational tissues by PMCA. *Sci. Rep.* **11**, 18385. <https://doi.org/10.1038/s41598-021-97737-y> (2021).
- Angers, R. C. *et al.* Chronic wasting disease prions in elk antler velvet. *Emerg. Infect. Dis.* **15**, 696–703. <https://doi.org/10.3201/eid1505.081458> (2009).
- Haley, N. J., Seelig, D. M., Zabel, M. D., Telling, G. C. & Hoover, E. A. Detection of CWD prions in urine and saliva of deer by transgenic mouse bioassay. *PLoS ONE* <https://doi.org/10.1371/journal.pone.0004848> (2009).
- Davenport, K. A. *et al.* Comparative analysis of prions in nervous and lymphoid tissues of chronic wasting disease-infected cervids. *J. Gen. Virol.* **99**, 753–758. <https://doi.org/10.1099/jgv.0.001053> (2018).
- Denkers, N. D. *et al.* Very low oral exposure to prions of brain or saliva origin can transmit chronic wasting disease. *PLoS ONE* <https://doi.org/10.1371/journal.pone.0237410> (2020).
- Morales, R. *et al.* Reduction of prion infectivity in packed red blood cells. *Biochem. Biophys. Res. Commun.* **377**, 373–378. <https://doi.org/10.1016/j.bbrc.2008.09.141> (2008).

37. Johnson, C. J., Aiken, J. M., McKenzie, D., Samuel, M. D. & Pedersen, J. A. Highly efficient amplification of chronic wasting disease agent by protein misfolding cyclic amplification with beads (PMCA). *PLoS ONE* **7**, e35383. <https://doi.org/10.1371/journal.pone.0035383> (2012).
38. Haley, N. J. *et al.* Cross-validation of the RT-QuIC assay for the antemortem detection of chronic wasting disease in elk. *Prion* **14**, 47–55. <https://doi.org/10.1080/19336896.2020.1716657> (2020).
39. Davenport, K. A., Hoover, C. E., Denkers, N. D., Mathiason, C. K. & Hoover, E. A. Modified protein misfolding cyclic amplification overcomes real-time quaking-induced conversion assay inhibitors in deer saliva to detect chronic wasting disease prions. *J. Clin. Microbiol.* <https://doi.org/10.1128/jcm.00947-18> (2018).
40. Orru, C. D., Wilham, J. M., Vascellari, S., Hughson, A. G. & Caughey, B. New generation QuIC assays for prion seeding activity. *Prion* **6**, 147–152. <https://doi.org/10.4161/pri.19430> (2012).
41. Concha-Marambio, L. *et al.* Detection of prions in blood from patients with variant Creutzfeldt–Jakob disease. *Sci. Transl. Med.* **8**, 370ra183. <https://doi.org/10.1126/scitranslmed.aaf6188> (2016).
42. Lacroux, C. *et al.* Preclinical detection of variant CJD and BSE prions in blood. *Plos. Pathog.* <https://doi.org/10.1371/journal.ppat.1004202> (2014).
43. Fox, K. A., Jewell, J. E., Williams, E. S. & Miller, M. W. Patterns of PrPCWD accumulation during the course of chronic wasting disease infection in orally inoculated mule deer (*Odocoileus hemionus*). *J. Gen. Virol.* **87**, 3451–3461. <https://doi.org/10.1099/vir.0.81999-0> (2006).
44. Wilham, J. M. *et al.* Rapid end-point quantitation of prion seeding activity with sensitivity comparable to bioassays. *Plos. Pathog.* **6**, e1001217. <https://doi.org/10.1371/journal.ppat.1001217> (2010).
45. Johnson, C. J., Aiken, J. M., McKenzie, D., Samuel, M. D. & Pedersen, J. A. Highly efficient amplification of chronic wasting disease agent by protein misfolding cyclic amplification with beads (PMCA). *PLoS ONE* <https://doi.org/10.1371/journal.pone.0035383> (2012).
46. Otero, A., Velasquez, C. D., Aiken, J. & McKenzie, D. White-tailed deer S96 prion protein does not support stable in vitro propagation of most common CWD strains. *Sci. Rep.* <https://doi.org/10.1038/s41598-021-90606-8> (2021).
47. Plummer, I. H., Johnson, C. J., Chesney, A. R., Pedersen, J. A. & Samuel, M. D. Mineral licks as environmental reservoirs of chronic wasting disease prions. *PLoS ONE* <https://doi.org/10.1371/journal.pone.0196745> (2018).
48. Johnson, C. J., Pedersen, J. A., Chappell, R. J., McKenzie, D. & Aiken, J. M. Oral transmissibility of prion disease is enhanced by binding to soil particles. *Plos. Pathog.* **3**, 874–881. <https://doi.org/10.1371/journal.ppat.0030093> (2007).
49. Miller, M. W., Williams, E. S., Hobbs, N. T. & Wolfe, L. L. Environmental sources of prion transmission in mule deer. *Emerg. Infect. Dis.* **10**, 1003–1006. <https://doi.org/10.3201/eid1006.040010> (2004).
50. Dantas-Torres, F. Biology and ecology of the brown dog tick, *Rhipicephalus sanguineus*. *Parasit. Vectors* **3**, 26. <https://doi.org/10.1186/1756-3305-3-26> (2010).
51. Gilbertson, M. L. J. *et al.* Cause of death, pathology, and chronic wasting disease status of white-tailed deer mortalities in Wisconsin. *J. Wildlife. Dis.* **58**, 803–815 (2022).
52. Soares, S. F., Louly, C. C., Marion-Poll, F., Ribeiro, M. F. & Borges, L. M. Study on cheliceral sensilla of the brown dog tick *Rhipicephalus sanguineus* (Latreille, 1806) (Acari: Ixodidae) involved in taste perception of phagostimulants. *Acta Trop.* **126**, 75–83. <https://doi.org/10.1016/j.actatropica.2013.01.006> (2013).
53. Burgener, K. R., Lichtenberg, S. S., Storm, D. J., Walsh, D. & Pedersen, J. A. Diagnostic testing of chronic wasting disease in white-tailed deer (*Odocoileus virginianus*) by RT-QuIC using skin samples. *PLoS ONE* **17**(11), e0274531. <https://doi.org/10.1371/journal.pone.0274531> (2021).
54. Metrick, M. A. 2nd. *et al.* Million-fold sensitivity enhancement in proteopathic seed amplification assays for biospecimens by Hofmeister ion comparisons. *Proc. Natl. Acad. Sci. USA* <https://doi.org/10.1073/pnas.1909322116> (2019).
55. Orru, C. D. *et al.* RT-QuIC assays for prion disease detection and diagnostics. *Methods Mol. Biol.* **1658**, 185–203. [https://doi.org/10.1007/978-1-4939-7244-9\\_14](https://doi.org/10.1007/978-1-4939-7244-9_14) (2017).
56. Browning, S. R. *et al.* Transmission of prions from mule deer and elk with chronic wasting disease to transgenic mice expressing cervid PrP. *J. Virol.* **78**, 13345–13350. <https://doi.org/10.1128/JVI.78.23.13345-13350.2004> (2004).
57. Green, M. R. & Sambrook J. in *Molecular cloning: A laboratory manual* Vol. 1 Ch. 15, 59–60 (Cold Spring Harbor Laboratory Press, 2012).
58. Raudabaugh, D. B. *et al.* County-wide assessments of Illinois white-tailed deer (*Odocoileus virginianus*) prion protein gene variation using improved primers and potential implications for management. *PLoS ONE* **17**, e0274640 (2022).
59. Haley, N., Donner, R., Merrett, K., Miller, M. & Senior, K. Selective breeding for disease-resistant PRNP variants to manage chronic wasting disease in farmed whitetail deer. *Genes* **12**, 1396 (2021).
60. Keeler, S. P., Bernarsky, N. L., Huffman, J. E. & Roscoe, D. E. A survey of the prion protein gene heterogeneity in New Jersey white-tailed deer (*Odocoileus virginianus*). *J. Pac. Acad. Sci.* **85**, 183–187 (2011).
61. Kramm, C., Soto, P., Nichols, T. A. & Morales, R. Chronic wasting disease (CWD) prion detection in blood from pre-symptomatic white-tailed deer harboring PRNP polymorphic variants. *Sci. Rep.* **10**, 19763. <https://doi.org/10.1038/s41598-020-75681-7> (2020).
62. Akaïke, H. A new look at the statistical model identification. *IEEE Trans. Automat. Control.* **19**, 716–723 (1974).
63. Inzalaco, H. N. & Lichtenberg, S. S. Ticks harbor and excrete chronic wasting disease prions. *US Geol. Surv. Data Release* <https://doi.org/10.5066/P9CAMSWN> (2023).

## Acknowledgements

This work was supported by the Wisconsin Department of Natural Resources (37000-0000009433 and 37000-0000010649), United States Geological Survey (G19AC00394), and National Institutes of Health (NIH/NIAID 1R01AI132695). We would like to thank Drs. Lyric Bartholomay and Susan Paskewitz for their guidance on tick rearing and artificial membrane feeding. We also thank Lisa Coburn from the Oklahoma State University Tick Rearing Facility for guidance on humidity chamber setup and maintenance and to Kevin Wallenfang with the Wisconsin Department of Natural Resources for helping coordinate the collection of samples from hunter-harvested wild WTD. Any use of trade, firm, or product names is for descriptive purposes only and does not imply endorsement by the U.S. Government.

## Author contributions

Conception and design of the work: H.N.I., S.S.L., J.A.P.; acquisition, analysis, and interpretation of the RT-QuIC data: H.N.I., S.S.L., acquisition, analysis, and interpretation of the data PMCA data: F.B.R. and R.M., resources and funding: J.A.P.; writing the original draft: H.N.I., revision and edition of the final manuscript: H.N.I., W.C.T., S.S.L., D.J.S., D.P.W., R.M., F.B.R., J.A.P. J.A.P. was a critical component of preparing this study but passed away before the final version was complete; all other authors approved and agreed to the submitted version of the present manuscript.

### Competing interests

R.M. is listed as an inventor in one patent related to the PMCA technology. H.N.I, F.B.R., S.S.L, J.A.P, D.J.S., D.P.W., and W.C.T. have no conflicts to declare for this study.

### Additional information

**Supplementary Information** The online version contains supplementary material available at <https://doi.org/10.1038/s41598-023-34308-3>.

**Correspondence** and requests for materials should be addressed to H.N.I.

**Reprints and permissions information** is available at [www.nature.com/reprints](http://www.nature.com/reprints).

**Publisher's note** Springer Nature remains neutral with regard to jurisdictional claims in published maps and institutional affiliations.



**Open Access** This article is licensed under a Creative Commons Attribution 4.0 International License, which permits use, sharing, adaptation, distribution and reproduction in any medium or format, as long as you give appropriate credit to the original author(s) and the source, provide a link to the Creative Commons licence, and indicate if changes were made. The images or other third party material in this article are included in the article's Creative Commons licence, unless indicated otherwise in a credit line to the material. If material is not included in the article's Creative Commons licence and your intended use is not permitted by statutory regulation or exceeds the permitted use, you will need to obtain permission directly from the copyright holder. To view a copy of this licence, visit <http://creativecommons.org/licenses/by/4.0/>.

© United States Geological Survey Work (USGS) 2023